SLAC-PUB-7937
June 1998

Renormalization of Supersymmetric Theories

By Damien M. Pierce

Presented at Theoretical Advanced Study Institute in Elementary Particle Physics (TASI 97): Supersymmetry, Supergravity and Supercolliders, 6/1/97—6/7/97, Boulder, CO, USA

Stanford Linear Accelerator Center, Stanford University, Stanford, CA 94309

Work supported by Department of Energy contract DE–AC03–76SF00515.

RENORMALIZATION OF SUPERSYMMETRIC THEORIES

DAMIEN M. PIERCE
Stanford Linear Accelerator Center
Stanford University
Stanford, CA 94309, USA
E-mail: pierce@slac.stanford.edu

We review the renormalization of the electroweak sector of the standard model. The derivation also applies to the minimal supersymmetric standard model. We discuss regularization, and the relation between the threshold corrections and the renormalization group equations. We consider the corrections to many precision observables, including M_W and $\sin^2\theta^{\rm eff}$. We show that global fits to the data exclude regions of supersymmetric model parameter space and lead to lower bounds on superpartner masses.

1 Introduction

1.1 The standard model and beyond

Over the past decade we have seen the standard model (SM) tested with increasing precision by a large number of experiments. It is quite remarkable that as the measurements become more accurate and encompass more observables, the standard model is repeatedly confirmed to greater precision. When discrepancies are found, they always seem to evaporate with subsequent data and/or analyses. From the point of view of precision measurements there is no need for physics beyond the standard model.

With so much direct experimental evidence confirming the standard model (and no evidence of discrepancies[1]) it might appear somewhat mysterious that so much time and effort is spent studying models beyond the standard model. There are many reasons why people believe the standard model with a light Higgs boson is not the whole story. Many agree that new physics near the electroweak scale is necessary in order to resolve the hierarchy problem. They point out that in order for the huge hierarchy between the electroweak and Planck scales to exist the parameters in the Higgs sector of the standard model must be tuned to one part in 10^{34}. New physics near the electroweak scale can stabilize or obviate this hierarchy. As the scale of new physics is raised above the TeV scale, either a new (albeit much less severe) hierarchy problem arises or there are problems with perturbative unitarity. Another major reason to consider physics beyond the standard model is in order to find a simpler or unified theory which offers an explanation for the standard model symmetries, matter content, and/or gives some framework for understanding the values of

the 18 standard model input parameters.

Models of physics beyond the standard model can for the most part be divided into two classes, which are distinguished by their implementation of electroweak symmetry breaking. These are technicolor theories and supersymmetry. The simplest (and, it turns out, unviable) technicolor models operate in many respects like a scaled-up version of QCD. Such models typically encounter problems related to the fermion mass hierarchy, flavor changing neutral currents, electroweak precision tests, and/or light pseudoscalars. To avoid this plethora of pitfalls, rather large, complicated, and seemingly *ad hoc* models must be invoked.

Supersymmetry, on the other hand, does not suffer from any of the previously mentioned problems. In fact, due to the decoupling nature of supersymmetric corrections, the minimal supersymmetric standard model (MSSM) with a heavy ($\sim$ 1 TeV) superpartner spectrum is indistinguishable from the standard model in all weak-scale experiments. In this light, the success of the standard model can be also realized as the success of the MSSM.

The fact that the gauge couplings nearly unify in the MSSM [2] (but not the standard model) may be taken as indirect evidence for supersymmetric grand unified theories (GUTs). String theory is the only viable candidate for a theory of quantum gravity, and supersymmetry remains (for the most part) an essential element in the construction of sensible string theories. In some string models, low-energy supersymmetry is an unavoidable by-product. Gauge coupling unification can arise in string theory, with or without a GUT.

Another nice virtue of supersymmetry is related to electroweak symmetry breaking. In the standard model, electroweak symmetry breaking is accomplished by setting the Higgs mass parameter to the wrong-sign by hand. In popular supersymmetric models, however, the Higgs mass parameter has a positive value at an initial (high) scale. By virtue of radiative corrections the mass runs with the scale, and at the electroweak scale it has the wrong sign. This radiative breaking of electroweak symmetry is a rather generic feature of supersymmetric models.

While supersymmetric theories readily explain electroweak symmetry breaking, they introduce the problem of supersymmetry breaking. *A priori* there are hundreds of arbitrary new parameters in the supersymmetry-breaking Lagrangian. There are simple models of supersymmetry breaking which greatly reduce the number of parameters. For example, in the simplest gravity- and gauge-mediated models that we will consider, there are about 5 input parameters.

With this introduction, we are motivated to study in some detail the ramifications of low-energy supersymmetry. Radiative corrections play an essential

role in much of the discussion of supersymmetry phenomenology. In the next section we will pedagogically review renormalization of the electroweak sector of the standard model. This discussion applies to the MSSM as well. In the following section we discuss regularization, threshold corrections, and the renormalization group equations (RGEs). We apply these results when we discuss the global fit of electroweak data in the standard model and the MSSM in Sec. 4. A brief summary and conclusions are provided in Sec. 5.

2 Electroweak Renormalization

Renormalization remains a cornerstone of particle physics. In any model of particle physics, whether the standard model or beyond, if radiative corrections are to be taken into account some renormalization procedure must be implemented. Here we review the standard technique of counterterm renormalization. We will focus on the renormalization necessary to calculate the supersymmetric corrections to electroweak observables. For this we need not consider full gauge-sector renormalization (ghosts; gauge-fixing). For a more complete treatment see Ref. [3].

We first introduce the counterterms, and then discuss the renormalization conditions which determine them. In the following section we consider the calculation of the counterterms (and Feynman diagrams in general) by discussing regularization and Passarino-Veltman functions.

The renormalization procedure is straightforward. We start in each case with the bare Lagrangian, which consists of bare parameters (bare masses and couplings) and bare fields. We write this in terms of the renormalized parameters and fields. For example, the bare mass m_b and coupling e_b are replaced by the renormalized parameters m and e, and the associated counterterms, δm and δe,

$$m_b = m + \delta m \ , \qquad e_b = e + \delta e \ .$$

The bare fields are equal to the renormalized fields multiplied by a wave-function renormalization factor, *e.g.*

$$\phi_b = Z^{\frac{1}{2}} \phi \ .$$

The $Z^{\frac{1}{2}}$ factor is in general a matrix, mixing fields with the same quantum numbers into each other. After these replacements, we can separate the bare Lagrangian into the renormalized Lagrangian and the counterterm Lagrangian. The counterterm Lagrangian gives rise to new vertices, which lead to new graphs in each order of perturbation theory. These counterterm graphs cancel subdivergences in multiloop diagrams. At one-loop order, however, the counterterm vertices enter only in tree graphs. Hence, the one-loop renormalization

procedure is quite simple, and amounts to adding the one-loop diagram contribution to the tree-level (bare) Lagrangian contribution. In the last step of the renormalization procedure we apply the renormalization conditions. The renormalization conditions determine the counterterms and the physical meaning of the renormalized parameters.

For mass and wave-function renormalization, it is most natural to impose the on-shell renormalization conditions. In this case the renormalized mass is the pole mass (*i.e.* the experimentally measured mass). The on-shell renormalization conditions consist of two parts:

a) the renormalized mass is the real part of the pole of the propagator, (1)

b) the real part of the residue of the pole is unity. (2)

In the general case the inverse propagator is a matrix. The bosonic form is

$$D^{-1}(p^2) = \begin{pmatrix} p^2 - m_{11}^2 + \Pi_{11}(p^2) & -m_{12}^2 + \Pi_{12}(p^2) & \cdots \\ -m_{21}^2 + \Pi_{21}(p^2) & p^2 - m_{22}^2 + \Pi_{22}(p^2) & \cdots \\ \vdots & \vdots & \cdots \end{pmatrix} . \quad (3)$$

Here p^2 is the external momenta-squared, m_{ij} is the tree-level (bare) mass matrix and $\Pi_{ij}(p^2)$ is the one-loop self-energy. The poles p_i^2 are determined from

$$\mathrm{Det}\left(D^{-1}(p^2)\right) = 0 \ ,$$

and the pole masses are $m_i^2 = \mathcal{R}e\,(p_i^2)$.

Scalar mass and wave-function renormalization provides the simplest example. The quadratic part of the bare Lagrangian is

$$\begin{aligned} \mathcal{L} &= \partial_\mu \phi_b^* \partial^\mu \phi_b - m_b^2 \phi_b^* \phi_b \\ &= Z_\phi \partial_\mu \phi^* \partial^\mu \phi - Z_\phi (m^2 + \delta m^2) \phi^* \phi \ . \end{aligned} \quad (4)$$

So, the bare inverse propagator can be read off, and at one-loop level we simply add the self-energy to obtain the renormalized inverse propagator,

$$D^{-1}(p^2) = Z_\phi p^2 - Z_\phi (m^2 + \delta m^2) + \Pi(p^2) \ .$$

The real part of the pole of the propagator is

$$\mathcal{R}e\,(p^2) = m^2 + \delta m^2 - Z_\phi^{-1} \mathcal{R}e\,\Pi(p^2) \ .$$

The on-shell renormalization condition requires $\mathcal{R}e\,(p^2) = m^2$. This implies

$$\delta m^2 = Z_\phi^{-1} \mathcal{R}e\,\Pi(p^2) \ . \quad (5)$$

At $\mathcal{O}(\alpha)$ we can set $Z_\phi^{-1} = 1$ and $p^2 = m^2$ in this equation, to obtain

$$\delta m^2 = \mathcal{R}e\,\Pi(m^2)\ . \tag{6}$$

The residue of the pole of the propagator is

$$\mathrm{res}\left(D(p^2)\right) = Z_\phi + \Pi'(p^2)\ . \tag{7}$$

The prime denotes the derivative with respect to p^2. The second part of the on-shell renormalization conditions requires that the real part of the residue be equal to unity,

$$Z_\phi + \mathcal{R}e\,\Pi'(p^2) = 1\ . \tag{8}$$

Again, at $\mathcal{O}(\alpha)$ we can replace the complex pole p^2 by the real part, the renormalized mass, so that

$$Z_\phi = 1 - \mathcal{R}e\,\Pi'(m^2)\ . \tag{9}$$

Next we consider gauge-boson mass and wave-function renormalization. In this case the inverse propagator has a longitudinal and transverse part,

$$D_{\mu\nu}(p^2) = \left(-g_{\mu\nu} + \frac{p_\mu p_\nu}{p^2}\right)\ D^T(p^2) + \frac{p_\mu p_\nu}{p^2}\ D^L(p^2)\ . \tag{10}$$

Only the transverse part of the propagator contributes to physical processes. Correspondingly, only the transverse part of the one-loop self energy will appear in the corrections.

The gauge boson renormalization is quite similar to the scalar case we just considered. In the standard model γ-Z mixing introduces a slight complication. The quadratic part of the bare Lagrangian involving γ and Z is

$$\mathcal{L} = (A_b^\mu \quad Z_b^\mu) \begin{pmatrix} \Box & 0 \\ 0 & \Box - M_{Z_b}^2 \end{pmatrix} \begin{pmatrix} A_{\mu_b} \\ Z_{\mu_b} \end{pmatrix}\ , \tag{11}$$

where $\Box$ denotes the D'Alembertian. As usual we rewrite this in terms of the renormalized parameters and fields,

$$\begin{aligned}
&\mathcal{L} = \\
&(A^\mu \quad Z^\mu) \begin{pmatrix} Z_{\gamma\gamma}^{\frac{1}{2}} & Z_{Z\gamma}^{\frac{1}{2}} \\ Z_{\gamma Z}^{\frac{1}{2}} & Z_{ZZ}^{\frac{1}{2}} \end{pmatrix} \begin{pmatrix} \Box & 0 \\ 0 & \Box - M_Z^2 - \delta M_Z^2 \end{pmatrix} \begin{pmatrix} Z_{\gamma\gamma}^{\frac{1}{2}} & Z_{\gamma Z}^{\frac{1}{2}} \\ Z_{Z\gamma}^{\frac{1}{2}} & Z_{ZZ}^{\frac{1}{2}} \end{pmatrix} \begin{pmatrix} A^\mu \\ Z^\mu \end{pmatrix} \\
&= (A^\mu Z^\mu) \begin{pmatrix} Z_{\gamma\gamma}\Box & Z_{\gamma Z}^{\frac{1}{2}}\Box + Z_{Z\gamma}^{\frac{1}{2}}(\Box - M_Z^2 - \delta M_Z^2) \\ Z_{\gamma Z}^{\frac{1}{2}}\Box + Z_{Z\gamma}^{\frac{1}{2}}(\Box - M_Z^2 - \delta M_Z^2) & Z_{ZZ}(\Box - M_Z^2 - \delta M_Z^2) \end{pmatrix} \\
&\qquad\qquad \times \begin{pmatrix} A^\mu \\ Z^\mu \end{pmatrix}\ .
\end{aligned}$$

We have dropped some terms of $\mathcal{O}(\alpha^2)$ such as $(1 - Z_{\gamma\gamma}^{\frac{1}{2}}) Z_{\gamma Z}^{\frac{1}{2}}$. The inverse propagator may be read off as

$$D^{-1}(p^2) = \begin{pmatrix} Z_{\gamma\gamma} p^2 + \Pi_{\gamma\gamma}^T(p^2) & D_{\gamma Z}^{-1}(p^2) \\ D_{Z\gamma}^{-1}(p^2) & Z_{ZZ}(p^2 - M_Z^2 - \delta M_Z^2) + \Pi_{ZZ}^T(p^2) \end{pmatrix} , \quad (12)$$

where

$$D_{\gamma Z}^{-1}(p^2) = D_{Z\gamma}^{-1}(p^2) = Z_{\gamma Z}^{\frac{1}{2}} p^2 + Z_{Z\gamma}^{\frac{1}{2}}(p^2 - M_Z^2 - \delta M_Z^2) + \Pi_{\gamma Z}^T(p^2) , \quad (13)$$

and we added the transverse part of the gauge-boson self-energy, $\Pi^T(p^2)$.

We determine the counterterms by applying the on-shell renormalization conditions, (1–2), which in this case can be realized by [a]

$$\text{a)} \quad D_{\gamma\gamma}^{-1}(0) = 0 \quad (14)$$

$$\mathcal{R}e\, D_{ZZ}^{-1}(M_Z^2) = 0 \quad (15)$$

$$D_{\gamma Z}^{-1}(0) = \mathcal{R}e\, D_{\gamma Z}^{-1}(M_Z^2) = 0 \quad (16)$$

$$\text{b)} \quad \mathcal{R}e\, D_{\gamma\gamma}^{-1\,\prime}(0) = \mathcal{R}e\, D_{ZZ}^{-1\,\prime}(M_Z^2) = 1 \quad (17)$$

These determine the counterterms

$$\delta M_Z^2 = \mathcal{R}e\, \Pi_{ZZ}^T(M_Z^2) , \quad (18)$$

$$Z_{\gamma\gamma} = 1 - \mathcal{R}e\, \Pi_{\gamma\gamma}^{T'}(0) , \quad (19)$$

$$Z_{ZZ} = 1 - \mathcal{R}e\, \Pi_{ZZ}^{T'}(M_Z^2) , \quad (20)$$

$$Z_{\gamma Z}^{\frac{1}{2}} = -\mathcal{R}e\, \frac{\Pi_{\gamma Z}^T(M_Z^2)}{M_Z^2} , \quad (21)$$

$$Z_{Z\gamma}^{\frac{1}{2}} = \frac{\Pi_{\gamma Z}^T(0)}{M_Z^2} . \quad (22)$$

Note that no photon mass counterterm is required since the U(1) Ward identity ensures $\Pi_{\gamma\gamma}^T(0) = 0$. For the W-boson we find

$$\delta M_W^2 = \mathcal{R}e\, \Pi_{WW}^T(M_W^2) , \quad (23)$$

$$Z_{WW} = 1 - \mathcal{R}e\, \Pi_{WW}^{T'}(M_W^2) . \quad (24)$$

The final mass and wave-function renormalization we need to consider applies to fermion fields. Just as in the previous examples, we start by writing the

[a] We use the fact that a self-energy evaluated at zero external momentum is real.

bare Lagrangian, then substitute for the renormalized fields and mass. In general we will have mixing among the fields, so the masses and the wave-function renormalization constants will be matrices. The bare kinetic Lagrangian in the mass basis is [b]

$$\begin{aligned}\mathcal{L}_{\rm bare} &= i\,\overline{\psi}_{b_L}\partial\!\!\!/\psi_{b_L} + i\,\overline{\psi}_{b_R}\partial\!\!\!/\psi_{b_R} - \overline{\psi}_{b_L} m_b \psi_{b_R} - \overline{\psi}_{b_R} m_b \psi_{b_L} \\ &= i\,\overline{\psi}_L Z_L^{\frac{1}{2}\dagger}\partial\!\!\!/ Z_L^{\frac{1}{2}}\psi_L + i\,\overline{\psi}_R Z_R^{\frac{1}{2}\dagger}\partial\!\!\!/ Z_R^{\frac{1}{2}}\psi_R \\ &\quad - \overline{\psi}_L Z_L^{\frac{1}{2}\dagger}(m+\delta m) Z_R^{\frac{1}{2}}\psi_R - \overline{\psi}_R Z_R^{\frac{1}{2}\dagger}(m+\delta m) Z_L \psi_L \ ,\end{aligned}$$

where $\psi_{L,R} = (1 \mp \gamma_5)/2\ \psi$. From this expression we can read off the bare inverse propagator, and at one-loop we simply add the self-energy contribution $(\Sigma_L,\ \Sigma_R,\ \Sigma_S)$ to obtain the renormalized inverse propagator [c],

$$\begin{aligned}S_{ij}^{-1}(\not{p}) &= \left(Z_L^{\frac{1}{2}\dagger} Z_L^{\frac{1}{2}}\right)_{ij} \not{p} P_L + \left(Z_R^{\frac{1}{2}\dagger} Z_R^{\frac{1}{2}}\right)_{ij} \not{p} P_R \\ &\quad - (Z_{R\,ik}^{\frac{1}{2}\dagger} m_k Z_{L\,kj}^{\frac{1}{2}} + \delta m_i\,\delta_{ij}) P_L \\ &\quad - (Z_{L\,ik}^{\frac{1}{2}\dagger} m_k Z_{R\,kj}^{\frac{1}{2}} + \delta m_i\,\delta_{ij}) P_R \\ &\quad + \Sigma_{L\,ij}(p^2)\not{p} P_L + \Sigma_{R\,ij}(p^2)\not{p} P_R + \Sigma_{S\,ij}(p^2) P_L + \Sigma_{S\,ji}^*(p^2) P_R \ .\end{aligned}$$

We can define $Z_{L,R}^{\frac{1}{2}} \equiv 1 + \delta Z_{L,R}/2$. Then we have

$$\begin{aligned}S_{ij}^{-1}(\not{p}) &= \left[\delta_{ij} + \frac{1}{2}\left(\delta Z_L + \delta Z_L^\dagger\right)_{ij} + \Sigma_{L\,ij}(p^2)\right]\not{p} P_L \\ &\quad + \left[\delta_{ij} + \frac{1}{2}\left(\delta Z_R + \delta Z_R^\dagger\right)_{ij} + \Sigma_{R\,ij}(p^2)\right]\not{p} P_R \\ &\quad - \left[m_i\delta_{ij} + \frac{1}{2}\delta Z_{R\,ij}^\dagger m_j + \frac{1}{2} m_i \delta Z_{L\,ij} + \delta m_i\,\delta_{ij} - \Sigma_{S\,ij}(p^2)\right] P_L \\ &\quad - \left[m_i\delta_{ij} + \frac{1}{2}\delta Z_{L\,ij}^\dagger m_j + \frac{1}{2} m_i \delta Z_{R\,ij} + \delta m_i\,\delta_{ij} - \Sigma_{S\,ji}^*(p^2)\right] P_R \ .\end{aligned}$$

To apply the on-shell renormalization conditions it is convenient to introduce an on-shell spinor u which satisfies the equation of motion $(\not{p} - m)\,u = 0$. Recall that the on-shell renormalization conditions have two parts. The first

[b] Note in the mass basis m and δm are real and diagonal.

[c] We assumed hermiticity, which implies that $\Sigma_{L\,ii}$ and $\Sigma_{R\,ii}$ are real and $\Sigma_{S\,R} = \Sigma_{S\,L}^\dagger$. If the fermion under consideration is unstable the effective Lagrangian is not Hermitian.

part requires that the poles of the renormalized propagator are at the renormalized masses. A pole in the propagator corresponds to a vanishing column in the inverse propagator, when the spinor multiplies the inverse propagator on the right. We implement this condition by requiring

$$S_{ij}^{-1}(\not{p})u(m_j) = 0 \tag{25}$$

for all i, j. The second part of the on-shell renormalization conditions requires that the residues of the propagator poles are unity. Note that Eq. (25) only requires that the diagonal elements of the inverse propagator have the form $A(\not{p} - m_i)$. To ensure $A = 1$, we require

$$\frac{1}{\not{p} - m_i} S_{ii}^{-1}(\not{p})\, u(m_i) = u(m_i) \ . \tag{26}$$

From Eq. (25), with $i = j$, we have

$$\frac{1}{2}\left(\delta Z_L - \delta Z_R\right)_{ii} m_i - \delta m_i = -m_i \Sigma_{L\,ii}(m_i^2) - \Sigma^*_{S\,ii}(m_i^2) \ , \tag{27}$$

$$\frac{1}{2}\left(\delta Z_R - \delta Z_L\right)_{ii} m_i - \delta m_i = -m_i \Sigma_{R\,ii}(m_i^2) - \Sigma_{S\,ii}(m_i^2) \ . \tag{28}$$

The sum and difference give

$$\delta m_i = \frac{1}{2}\left[\Sigma_{L\,ii}(m_i^2) + \Sigma_{R\,ii}(m_i^2)\right] m_i + \mathcal{R}e\,\Sigma_{S\,ii}(m_i^2) \ , \tag{29}$$

$$\delta Z_{L\,ii} - \delta Z_{R\,ii} = \Sigma_{R\,ii}(m_i^2) - \Sigma_{L\,ii}(m_i^2) + \frac{2}{m_i}\,\mathcal{I}m\Sigma_{S\,ii}(m_i^2) \ . \tag{30}$$

With $i \neq j$, we find from Eq. (25)

$$\frac{1}{2}\delta Z_{L\,ij}\, m_j - \frac{1}{2} m_i\, \delta Z_{R\,ij} + \Sigma_{L\,ij}(m_j^2)\, m_j + \Sigma^*_{S\,ji}(m_j^2) = 0 \ , \tag{31}$$

$$\frac{1}{2}\delta Z_{R\,ij}\, m_j - \frac{1}{2} m_i\, \delta Z_{L\,ij} + \Sigma_{R\,ij}(m_j^2)\, m_j + \Sigma_{S\,ij}(m_j^2) = 0 \ . \tag{32}$$

This then determines

$$\delta Z_{L\,ij} = \tag{33}$$
$$\frac{2}{m_i^2 - m_j^2}\left[m_j^2 \Sigma_{L\,ij}(m_j^2) + m_i m_j \Sigma_{R\,ij}(m_j^2) + m_i \Sigma_{S\,ij}(m_j^2) + m_j \Sigma^*_{S\,ji}(m_j^2)\right] \ ,$$

$$\delta Z_{R\,ij} = \tag{34}$$
$$\frac{2}{m_i^2 - m_j^2}\left[m_j^2 \Sigma_{R\,ij}(m_j^2) + m_i m_j \Sigma_{L\,ij}(m_j^2) + m_j \Sigma_{S\,ij}(m_j^2) + m_i \Sigma^*_{S\,ji}(m_j^2)\right] \ .$$

Eq. (26) implies

$$\frac{1}{\not p - m_i}\Bigg[\frac{1}{2}\left(\delta Z_L + \delta Z_L^\dagger\right)_{ii}\not p - \frac{1}{2}\left(\delta Z_L^\dagger + \delta Z_R\right)_{ii} m_i \qquad (35)$$
$$-\delta m_i + \Sigma_{L\,ii}(p^2)\not p + \Sigma^*_{S\,ii}(p^2)\Bigg] u(m_i) = 0 \ ,$$
$$\frac{1}{\not p - m_i}\Bigg[\frac{1}{2}\left(\delta Z_R + \delta Z_R^\dagger\right)_{ii}\not p - \frac{1}{2}\left(\delta Z_R^\dagger + \delta Z_L\right)_{ii} m_i \qquad (36)$$
$$-\delta m_i + \Sigma_{R\,ii}(p^2)\not p + \Sigma_{S\,ii}(p^2)\Bigg] u(m_i) = 0 \ .$$

Taking the sum of these equations, and substituting δm_i from Eq. (29), we find

$$\frac{1}{\not p - m_i}\Bigg[\frac{1}{2}\left(\delta Z_L + \delta Z_L^\dagger + \delta Z_R + \delta Z_R^\dagger\right)_{ii}(\not p - m_i) \qquad (37)$$
$$+\Big(f(p^2)\not p - f(m_i^2)m_i\Big) + \Big(g(p^2) - g(m_i^2)\Big)\Bigg] u(m_i) = 0$$

where

$$f(p^2) = \Sigma_{L\,ii}(p^2) + \Sigma_{R\,ii}(p^2) \ , \qquad (38)$$
$$g(p^2) = 2\,\mathcal{R}e\,\Sigma_{S\,ii}(p^2) \ . \qquad (39)$$

Note that

$$\frac{1}{\not p - m_i}\Big(f(p^2)\not p - f(m_i^2)m_i\Big)u(m_i) = \Big(f(m_i^2) + 2m_i^2 f'(m_i^2)\Big)u(m_i) \ ,$$
$$\frac{1}{\not p - m_i}\Big(g(p^2) - g(m_i^2)\Big)u(m_i) = 2m_i g'(m_i^2)u(m_i) \ ,$$

where $f'(m^2) = \partial f(p^2)/\partial p^2|_{p^2=m^2}$. Eq. (30) implies

$$\left(\delta Z_R + \delta Z_R^\dagger\right)_{ii} = \left(\delta Z_L + \delta Z_L^\dagger\right)_{ii} + 2\left(\Sigma_L(m_i^2) - \Sigma_R(m_i^2)\right)_{ii} \ . \qquad (40)$$

Substituting this in Eq. (37), we find

$$\mathcal{R}e\ \delta Z_{L\,ii} = -\Sigma_{L\,ii}(m_i^2) - m_i^2\left(\Sigma'_{L\,ii}(m_i^2) + \Sigma'_{R\,ii}(m_i^2)\right) - 2m_i\,\mathcal{R}e\,\Sigma'_{S\,ii}(m_i^2) \ ,$$
$$\mathcal{R}e\ \delta Z_{R\,ii} = -\Sigma_{R\,ii}(m_i^2) - m_i^2\left(\Sigma'_{L\,ii}(m_i^2) + \Sigma'_{R\,ii}(m_i^2)\right) - 2m_i\,\mathcal{R}e\,\Sigma'_{S\,ii}(m_i^2) \ .$$

Note that the Lagrangian is invariant if we rotate both the left and right-handed fields $\psi_{L\,i}$, $\psi_{R\,i}$ by phases $e^{i\theta_i}$. This means that there is an arbitrariness in the diagonal wave-function renormalization constants. The on-shell renormalization conditions are still satisfied if we transform the δZ_{ii}'s as

$$\delta Z_{L\,ii} \to e^{i\theta_i}\delta Z_{L\,ii} \ , \qquad \delta Z_{R\,ii} \to e^{i\theta_i}\delta Z_{R\,ii} \ . \tag{41}$$

No physical results depend on this arbitrariness. This freedom allows us to choose the $\delta Z_{R\,ii}$ to be real. We then determine the imaginary part of $\delta Z_{L\,ii}$ from Eq. (30). We add it to the real part to obtain

$$\begin{aligned}\delta Z_{L\,ii} = -\Sigma_{L\,ii}(m_i^2) - m_i^2\left(\Sigma'_{L\,ii}(m_i^2) + \Sigma'_{R\,ii}(m_i^2)\right) \\ -2m_i\,\mathcal{R}e\,\Sigma'_{S\,ii}(m_i^2) + \frac{2}{m_i}\,\mathcal{I}m\Sigma_{S\,ii}(m_i^2) \ .\end{aligned} \tag{42}$$

The fermion renormalization constants are somewhat complicated. If one introduces the effective mixing matrices, which diagonalize the renormalized mass matrix, the wave-function renormalization takes a much simpler form. In particular, the off-diagonal wave-function renormalization constants (Eqs. (33–34)) are absorbed in the construction of the effective mixing matrices. See Ref. [4] for details.

We will be primarily interested in the e and μ lepton wave-function renormalization. In the standard model, and in the supersymmetric extensions we will consider, $\mathcal{I}m\,\Sigma_{S\,ii} = 0$. Also, there is no lepton mixing, and we can approximate $m_\ell = 0$. In this case the lepton wave-function renormalization takes the particularly simple form

$$\delta Z_L = -\Sigma_L(0) \ , \qquad \delta Z_R = -\Sigma_R(0) \ . \tag{43}$$

We will use Eq. (43) repeatedly.

It will be convenient to write the wave-function renormalization in the vector/axial-vector basis. Consider the wave-function renormalization of

$$\overline{\psi}_b\gamma_\mu(g_L P_L + g_R P_R)\psi_b = \overline{\psi}\gamma_\mu(Z_L g_L P_L + Z_R g_R P_R)\psi \ .$$

It is a simple exercise to show that

$$\overline{\psi}\gamma_\mu(Z_L g_L P_L + Z_R g_R P_R)\psi = \overline{\psi}\Big[(g_v Z_v + g_a Z_a) - (g_v Z_a + g_a Z_v)\gamma_5\Big]\psi \ ,$$

where

$$g_v = \frac{1}{2}(g_L + g_R) \ , \qquad g_a = \frac{1}{2}(g_L - g_R) \ , \tag{44}$$

$$Z_v = \frac{1}{2}(Z_L + Z_R) \ , \qquad Z_a = \frac{1}{2}(Z_L - Z_R) \ . \tag{45}$$

Note that $Z_v = 1 + \mathcal{O}(\alpha)$ and $Z_a = \mathcal{O}(\alpha)$. Hence, we introduce $\delta Z_v \equiv 1 - Z_v$ and $\delta Z_a \equiv Z_a$.

With these gauge-boson and fermion mass and wave-function renormalizations, it is straightforward to renormalize the electric charge. The bare Lagrangian contains the interaction terms

$$\begin{aligned}
\mathcal{L}_{\rm int} = \quad & -e_b Q\, \overline{\psi}_b \gamma_\mu \psi_b A_b^\mu - \overline{\psi}_b \gamma_\mu (g_{v\,b} - g_{a\,b}\gamma_5)\psi_b Z_b^\mu & (46)\\
= \; & -(e+\delta e)\, Q\; \overline{\psi}\gamma_\mu (Z_v - Z_a\gamma_5)\psi \left(Z_{\gamma\gamma}^{\frac{1}{2}} A_\mu + Z_{\gamma Z}^{\frac{1}{2}} Z^\mu \right) & (47)\\
& -\overline{\psi}\gamma_\mu \Big[(g_v Z_v + g_a Z_a) - (g_v Z_a + g_a Z_v)\gamma_5 \Big] \psi \left(Z_{ZZ}^{\frac{1}{2}} Z_\mu + Z_{Z\gamma}^{\frac{1}{2}} A^\mu \right) .
\end{aligned}$$

The terms involving A^μ are (dropping terms of $\mathcal{O}(\alpha^2)$),

$$\begin{aligned}
& -e\, A^\mu & (48)\\
& \overline{\psi}\,\gamma_\mu \left\{ \left[Q\left(1 + \frac{\delta e}{e} + \delta Z_v + \frac{1}{2}\delta Z_{\gamma\gamma}\right) + \frac{g_v}{e} Z_{Z\gamma}^{\frac{1}{2}} \right] - \left[Q\,\delta Z_a + \frac{g_a}{e} Z_{Z\gamma}^{\frac{1}{2}} \right]\gamma_5 \right\} \psi \; .
\end{aligned}$$

There are three form factors in the proper fermion-photon vertex,

$$\begin{aligned}
& i\Lambda_\mu(k^2, p_1^2, p_2^2) = & (49)\\
& -ie\left[V_1(k^2, p_1^2, p_2^2)\gamma_\mu - V_2(k^2, p_1^2, p_2^2)\gamma_\mu\gamma_5 + \frac{i\sigma_{\mu\nu}k^\nu}{2m_e} V_3(k^2, p_1^2, p_2^2) \right] .
\end{aligned}$$

We can read off the tree-level vertex from Eq. (48) and at one-loop we simply add the proper vertex to obtain the renormalized vertex

$$\begin{aligned}
& \Gamma_\mu(k^2, p_1^2, p_2^2) = & (50)\\
& -e\Bigg\{ \gamma_\mu \left[Q\left(1 + \frac{\delta e}{e} + \delta Z_v + \frac{1}{2}\delta Z_{\gamma\gamma}\right) + \frac{g_v}{e} Z_{Z\gamma}^{\frac{1}{2}} + V_1(k^2, p_1^2, p_2^2) \right] \\
& -\gamma_\mu\gamma_5 \left[Q\,\delta Z_a + \frac{g_a}{e} Z_{Z\gamma}^{\frac{1}{2}} + V_2(k^2, p_1^2, p_2^2) \right] \; + \; \frac{i\sigma_{\mu\nu}k^\nu}{2m_e} V_3(k^2, p_1^2, p_2^2) \Bigg\} .
\end{aligned}$$

The on-shell renormalization condition for the vertex requires

$$\Gamma_\mu(0, m_e^2, m_e^2) = -eQ\gamma_\mu - \frac{ie\sigma_{\mu\nu}k^\nu}{2m_e} V_3(0, m_e^2, m_e^2) \; , \qquad (51)$$

with the renormalized charge e equal to that measured in Thompson scattering, $e^2/4\pi = 1/137.065$. The absence of an axial-vector contribution in Eq. (51) is an automatic consequence of the axial-vector Ward identity,

$$e\; Q\; \delta Z_a + e\; V_2(0, m_e^2, m_e^2) = -g_a\, Z_{Z\gamma}^{\frac{1}{2}} \; . \qquad (52)$$

There is a corresponding vector Ward identity,

$$e\ Q\ \delta Z_v + e\ V_1(0, m_e^2, m_e^2) = -g_a\ Z_{Z\gamma}^{\frac{1}{2}}\ . \tag{53}$$

Diagramatically, these equations correspond to (ignoring the magnetic moment contribution)

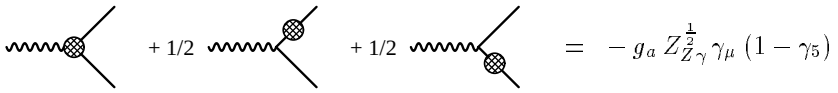

In QED the right hand side vanishes ($Z_{Z\gamma}^{\frac{1}{2}} = 0$) and the usual QED Ward identity is realized. In SU(2)×U(1), one can consider the various contributions to the right hand side from the various particles in the loop. From Eq. (22), $Z_{Z\gamma}^{\frac{1}{2}} = \Pi_{\gamma Z}^T(0)/M_Z^2$. At one-loop level, all the contributions to $\Pi_{\gamma Z}^T(0)$ vanish save one, that of the W-boson. This is true in any model with the standard model gauge symmetry. Hence, in the MSSM $\Pi_{\gamma Z}^T(0)$ has the same value as in the standard model.

If we substitute Eq. (53) into Eq. (50), we can write the on-shell vector coupling as

$$-eQ\gamma_\mu\left[1 + \frac{\delta e}{e} + \frac{1}{2}\delta Z_{\gamma\gamma} + \frac{g_v - g_a}{Qe} Z_{Z\gamma}^{\frac{1}{2}}\right] \tag{54}$$

which is equal to $-eQ\gamma_\mu$ by the renormalization condition Eq. (51). Hence,

$$\frac{\delta e}{e} = -\frac{1}{2}\delta Z_{\gamma\gamma} - \frac{g_v - g_a}{Qe} Z_{Z\gamma}^{\frac{1}{2}} \tag{55}$$

$$= \frac{1}{2}\Pi_{\gamma\gamma}^{T\prime}(0) + \frac{s}{c}\frac{\Pi_{\gamma Z}^T(0)}{M_Z^2}\ , \tag{56}$$

where s (c) is the sin (cos) of the weak mixing angle. It is customary to define $\Delta\alpha = \delta\alpha/\alpha = 2\delta e/e$.

Note that the vector Ward identity, Eq. (53), ensures that the renormalization of the electric charge is universal, *i.e.* the flavor dependent wave-function and vertex corrections drop out.

Building on these results, we can readily derive the relationships between the renormalized Fermi constant, the weak mixing angle, and the W-boson mass. The Fermi constant is measured most accurately in muon decay. By considering W-boson mediation at scales well below the W-boson mass, the bare effective Lagrangian is found to have the form

$$\mathcal{L}_{\rm eff} = \frac{G_{\mu\, b}}{\sqrt{2}}\ \overline{\psi}_b^{\nu_\mu}\gamma_\mu(1-\gamma_5)\psi_b^\mu\ \ \overline{\psi}_b^{e}\gamma^\mu(1-\gamma_5)\psi_b^{\nu_e}\ . \tag{57}$$

As usual this is equal to

$$\mathcal{L}_{\rm eff} = \frac{G_\mu + \delta G_\mu}{\sqrt{2}} Z_L^{\nu_\mu \frac{1}{2}} Z_L^{\mu \frac{1}{2}} Z_L^{e \frac{1}{2}} Z_L^{\nu_e \frac{1}{2}} \, \overline{\psi}^{\nu_\mu} \gamma_\mu (1-\gamma_5) \psi^{\mu} \, \overline{\psi}^{e} \gamma^\mu (1-\gamma_5) \psi^{\nu_e} \ . \quad (58)$$

The proper vertex function will in general contain other current bilinear products besides $(V-A)(V-A)$. However, in the SM and the MSSM these terms are suppressed by the small electron and muon masses, so they can be safely ignored. The vertex function contains the following contributions:

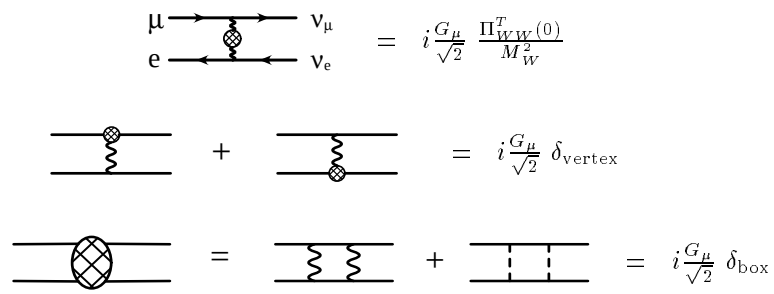

The renormalized coupling is then

$$\frac{G_\mu}{\sqrt{2}} \left[1 + \frac{\delta G_\mu}{G_\mu} + \frac{1}{2} \left(\delta Z_L^\mu + \delta Z_L^e + \delta Z_L^{\nu_\mu} + \delta Z_L^{\nu_e} \right) + \frac{\Pi^T_{WW}(0)}{M_W^2} + \delta_{\rm vertex} + \delta_{\rm box} \right] . \quad (59)$$

The muon decay rate was first calculated in the effective QED theory, where the photon corrections are taken into account, yielding

$$\tau_\mu^{-1} = \frac{G_\mu^2 m_\mu^5}{192\pi^3} \left(1 - \frac{8 m_e^2}{m_\mu^2} \right) \left[1 - \frac{\alpha}{2\pi} \left(\frac{25}{4} - \pi^2 \right) \right] . \quad (60)$$

The leading two-loop correction is included by evaluating α at the scale m_μ. It is customary to take Eq. (60) as the defining equation for G_μ. Then, from (59), we determine the counterterm δG_μ,

$$\frac{G_\mu}{\sqrt{2}} \left[1 + \frac{\delta G_\mu}{G_\mu} + \frac{1}{2} \left(\delta Z_L^\mu + \delta Z_L^e + \delta Z_L^{\nu_\mu} + \delta Z_L^{\nu_e} \right) + \frac{\Pi^T_{WW}(0)}{M_W^2} + \delta_{\rm vertex} + \delta_{\rm box} \right] = \frac{G_\mu}{\sqrt{2}} \left[1 + \delta_{\rm QED} \right] . \quad (61)$$

$\delta_{\rm QED}$ includes the photon correction in the effective theory,

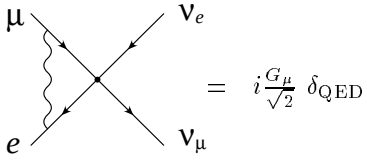

Hence, we have

$$\frac{\delta G_\mu}{G_\mu} = -\frac{\Pi^T_{WW}(0)}{M_W^2} - \delta_{VB} \tag{62}$$

where δ_{VB} denotes the non-QED wave-function, vertex, and box-diagram corrections,

$$\delta_{VB} = \frac{1}{2}\left(\delta Z_L^\mu + \delta Z_L^e + \delta Z_L^{\nu_\mu} + \delta Z_L^{\nu_e}\right) + \delta_{\rm vertex} + \delta_{\rm box} - \delta_{\rm QED} \ . \tag{63}$$

The superpartner contributions to δ_{VB} are given in Refs. [5,6].

We now have all the ingredients necessary to determine the renormalized weak mixing angle. The tree-level formula applies to the bare parameters,

$$\sqrt{2}\,G_{\mu_b} = \frac{\pi\alpha_b}{M^2_{Z_b} s_b^2 c_b^2} \ .$$

Replacing the bare parameters by the renormalized ones plus the counterterms, we find

$$\sqrt{2}\,(G_\mu + \delta G_\mu) = \frac{\pi\,\alpha\,(1+\Delta\alpha)}{(M_Z^2 + \delta M_Z^2)(s^2+\delta s^2)(c^2+\delta c^2)} \ . \tag{64}$$

Expanding to first order, and using $\delta c^2 = -\delta s^2$, we have

$$s^2c^2\left[1 + \delta s^2\left(\frac{c^2-s^2}{c^2 s^2}\right)\right] = \frac{\pi\alpha}{\sqrt{2}\,G_\mu M_Z^2}\left[1 + \Delta\alpha - \frac{\delta M_Z^2}{M_Z^2} - \frac{\delta G_\mu}{G_\mu}\right] \ . \tag{65}$$

Because of the on-shell renormalization conditions we have applied, the renormalized parameters on the right hand side of this equation include the electric coupling measured in Thompson scattering, the physical Z-boson pole mass measured at LEP, and the Fermi constant determined from the measurement of the muon lifetime. All of these physical quantities have corresponding counterterms. Plugging in the counterterms from Eqs. (18), (56) and (62), we

have

$$s^2c^2\left[1+\delta s^2\left(\frac{c^2-s^2}{c^2s^2}\right)\right]= \tag{66}$$

$$\frac{\pi\alpha}{\sqrt{2}\,G_\mu M_Z^2}\left[1+\Pi^{T\prime}_{\gamma\gamma}(0)+2\frac{s}{c}\frac{\Pi^T_{\gamma Z}(0)}{M_Z^2}-\mathcal{R}e\,\frac{\Pi^T_{ZZ}(M_Z^2)}{M_Z^2}+\frac{\Pi^T_{WW}(0)}{M_W^2}+\delta_{VB}\right]\ .$$

We now specify a meaning for s^2 at one-loop level. This results in a renormalization condition which determines the counterterm δs^2.

All the counterterms we have encountered thus far have both "finite" and "infinite" parts. In the calculation of Feynman diagrams one encounters divergences. A regularization method must be employed to control these divergences. Dimensional reduction is a natural regulator in supersymmetric theories, as will be discussed in the next section. In dimensional reduction the integrals are made finite by continuing spacetime to $n = 4-2\epsilon$ dimensions. Then, the divergences appear as poles in $1/\epsilon$. We can define a renormalized quantity by requiring its counterterm to be purely "infinite", *i.e.* proportional to $1/\epsilon$. The renormalized quantity is referred to as a $\overline{\rm DR}$ parameter [d], and depends on the $\overline{\rm DR}$ renormalization scale Q. From Eq. (66) we find the $\overline{\rm DR}$ renormalized weak mixing angle,

$$\hat{s}^2(Q^2)\hat{c}^2(Q^2)=\frac{\pi\alpha}{\sqrt{2}\,G_\mu M_Z^2}\left[1+\Delta\hat{\alpha}-\mathcal{R}e\,\frac{\hat{\Pi}^T_{ZZ}(M_Z^2)}{M_Z^2}+\frac{\hat{\Pi}^T_{WW}(0)}{M_W^2}+\hat{\delta}_{VB}\right]\ , \tag{67}$$

where the hat signifies $\overline{\rm DR}$ renormalization. We define

$$\Delta\hat{r}_Z=\Delta\hat{\alpha}-\mathcal{R}e\,\frac{\hat{\Pi}^T_{ZZ}(M_Z^2)}{M_Z^2}+\frac{\hat{\Pi}^T_{WW}(0)}{M_W^2}+\hat{\delta}_{VB}\ . \tag{68}$$

The leading irreducible corrections are correctly resummed by including the correction $\Delta\hat{r}_Z$ as [7]

$$\hat{s}^2\hat{c}^2=\frac{\pi\alpha}{\sqrt{2}\,G_\mu M_Z^2}\left[\frac{1}{1-\Delta\hat{r}_Z}\right]\ . \tag{69}$$

In particular, the largest correction is $\Delta\alpha$, and this form corresponds to the solution of the one-loop electric charge renormalization group equation.

To calculate the W-boson mass we introduce a $\overline{\rm DR}$ version of the ρ parameter,

$$\hat{\rho}=\frac{1}{\hat{c}^2}\frac{M_W^2}{M_Z^2}=\frac{\hat{M}_Z^2}{\hat{M}_W^2}\frac{M_W^2}{M_Z^2}=1+\Delta\hat{\rho}\ . \tag{70}$$

[d] The bar in $\overline{\rm DR}$ signifies that the $1/\epsilon$ pole is subtracted along with the universal integral artifacts $\ln 4\pi-\gamma_E$, where $\gamma_E=0.577216...$ is Euler's constant.

Using $\hat{M}_W^2 = M_W^2 + \mathcal{R}e\,\hat{\Pi}^T_{WW}(M_W^2)$ and $\hat{M}_Z^2 = M_Z^2 + \mathcal{R}e\,\hat{\Pi}^T_{ZZ}(M_Z^2)$, we find

$$\Delta\hat{\rho} = \mathcal{R}e\left[\frac{\hat{\Pi}^T_{ZZ}(M_Z^2)}{M_Z^2} - \frac{\hat{\Pi}^T_{WW}(M_W^2)}{M_W^2}\right] . \tag{71}$$

Defining

$$c_0^2 = \frac{1}{2}\left(1 + \sqrt{1 - \frac{4\pi\alpha}{\sqrt{2}\,G_\mu M_Z^2}}\right) , \tag{72}$$

we can expand Eq. (69) to obtain

$$\hat{c}^2 = c_0^2\left(1 - \frac{s_0^2}{c_0^2 - s_0^2}\Delta\hat{r}_Z\right) . \tag{73}$$

Then, using $M_W^2 = \hat{c}^2\hat{\rho}M_Z^2$, we find the prediction for the W-boson pole mass,

$$M_W^2 = \frac{c_0^2 M_Z^2}{1 - \Delta\hat{\rho} + \frac{s_0^2}{c_0^2 - s_0^2}\Delta\hat{r}_Z} . \tag{74}$$

Since the W-boson mass is a physical quantity, the correction is independent of the renormalization scheme to the order in which we are working. In particular, $\Delta\rho + s_0^2/(s_0^2 - c_0^2)\Delta r_Z$ is a physical observable. This combination of terms is gauge invariant, renormalization scale independent, and is the same whether hatted or unhatted.

3 Regularization, threshold corrections, and the RGEs

We have determined the mass, wave-function and electric charge counterterms by applying the on-shell renormalization conditions. These counterterms are comprised of two, three, and four-point diagrams corresponding to the various physical processes which are used to measure the input parameters. In supersymmetric models with the standard model gauge symmetry (*e.g.* the MSSM), the various diagrams receive extra contributions from the superpartners, but the forms of the counterterms remain unchanged.

The divergences which arise in calculating the counterterms and other Feynman diagrams must be regulated. In order to preserve the Ward (or Slavnov-Taylor) identities, and to avoid spurious complications, the regularization method employed should preserve the symmetries of the bare Lagrangian, even if they are spontaneously broken. Dimensional regularization respects gauge symmetry, so it is widely used as a regulator of gauge theories. In dimensional regularization spacetime is continued to $n = 4 - 2\epsilon$ dimensions. For

$n < 4$ it is clear that, for example, the integral

$$\int \frac{d^n k}{k^4}$$

is ultraviolet convergent. The divergences appear as simple poles in ϵ.

In dimensional regularization [8] (known variously as 'naive dimensional reduction', DIMR, or DREG) the dimensionality of spacetime and the (non-scalar) fields is continued to n-dimensions. Thus, the index of the gauge field A_μ runs from 0 to $n-1$. The Dirac algebra is n-dimensional, so, for example, $\gamma_\mu \gamma^\mu = n$, $\gamma_\mu \gamma_\nu \gamma^\mu = (2-n)\gamma_\nu$, and so on.

Continuing the dimensionality of the fields to n dimensions poses problems in supersymmetric theories. Supersymmetry requires equal numbers of on-shell bosonic and fermionic degrees of freedom in a multiplet. Continuing a four dimensional gauge supermultiplet to n dimensions will spoil this equality, so naive dimensional regularization (*e.g.* $\overline{\rm MS}$) breaks supersymmetry. One must add counterterms order by order in perturbation theory to restore supersymmetry. A new regularization method, called dimensional reduction, was invented for supersymmetric theories. In dimensional reduction [9] (DRED), spacetime is continued to n dimensions while the fields remain unchanged. Hence, the index on the gauge field runs from 0 to 3, and the Dirac algebra is 4 dimensional. There are potential problems with dimensional reduction [10]. Ambiguities appear in calculations using dimensional reduction at high orders in perturbation theory. It is unknown whether these ambiguities show up in calculations of corrections to physical observables. Even if they did, there may exist a consistent prescription which gives correct and unambiguous results. Also, it appears that the standard mass factorization in QCD is violated in dimensional reduction [11,12]. The situation is unclear as there has not yet been a complete investigation of the handling of collinear and infrared singularities in massive QCD in dimensional reduction. We stress that for our purposes these potential problems are purely academic. It is clear that, for the superpartner corrections we are concerned with, dimensional reduction is a convenient and valid gauge symmetry and supersymmetry preserving regulator at one or two loop order. We will use dimensional reduction in what follows.

We applied the on-shell renormalization conditions to determine the mass, wave-function, charge and Fermi constant counterterms. As mentioned in the previous section, it is in some cases expedient to use minimal subtraction to define a renormalized quantity and its counterterm. In minimal subtraction, naive dimensional regularization is employed, and the counterterm is defined to be 'purely infinite', *i.e.* proportional to the pole $1/\epsilon^n$. Usually the subscript 'MS' is used to signify a minimally subtracted renormalized quantity.

In modified minimal subtraction, the counterterm is prescribed to contain the pole as well as the n-dimensional integral artifacts that always appear with the pole, $\ln 4\pi - \gamma_E$. The two most common uses of modified minimal subtraction are in the renormalization of the weak mixing angle and the strong coupling constant. Such renormalized quantities are not physical observables. They are model dependent and renormalization scale dependent. Contributions from heavy particles do not decouple in such quantities (one has to implement decoupling by hand). Nevertheless, they are process independent, and they can be useful in comparing the implications of different experimental measurements in a given model.

In supersymmetry we use dimensional reduction to regulate the integrals, and the subtracted quantities in supersymmetric modified minimal subtraction are referred to as $\overline{\rm DR}$ renormalized quantities. We use a hat to denote a $\overline{\rm DR}$ renormalized quantity.

Consider the electric charge. If we perform $\overline{\rm DR}$ subtraction on the bare charge we obtain the renormalized $\overline{\rm DR}$ charge,

$$\begin{aligned} e_b = e + \delta e \qquad \Rightarrow \qquad e_b - (\delta e)_\infty &= \hat{e}(Q^2) = e + \delta e - (\delta e)_\infty \\ &= e\left(1 + \frac{1}{2}\hat{\Pi}^{T\prime}_{\gamma\gamma}(0) + \frac{s}{c}\frac{\hat{\Pi}^T_{\gamma Z}(0)}{M_Z^2}\right) \ , \end{aligned} \tag{75}$$

where the ∞ subscript denotes the $(1/\epsilon + \ln 4\pi - \gamma_E)$ part.

3.1 One-loop integrals

We now discuss the calculation of Feynman diagrams. With $n \leq 3$ there is only one scalar function for each n-point diagram which needs to be determined to evaluate the one-loop Feynman integrals. All the various tensor integrals can be written in terms of the scalar functions. The functions are as defined by Passarino and Veltman [13], except we work in the metric $(1,-1,-1,-1)$ and in some cases we differ by a minus sign.

For the one-point diagram, we have

$$Q^{4-n}\int \frac{d^nq}{(2\pi)^n}\frac{1}{[q^2 - m^2 + i\varepsilon]} \equiv \frac{i}{16\pi^2}A_0(m^2) \ . \tag{76}$$

The renormalization scale Q is necessary in order to keep the n-dimensional coupling dimensionless. This integral is

$$A_0(m^2) = m^2\left(\frac{1}{\hat{\epsilon}} + 1 + \ln\frac{Q^2}{m^2}\right) \ , \tag{77}$$

where $1/\hat{\epsilon} = 1/\epsilon + \ln 4\pi - \gamma_E$. The scalar two-point integral is defined as

$$Q^{4-n} \int \frac{d^n q}{(2\pi)^n} \frac{1}{[q^2 - m_1^2 + i\varepsilon]\,[(q-p)^2 - m_2^2 + i\varepsilon]} \equiv \frac{i}{16\pi^2} B_0(p^2, m_1^2, m_2^2) \ . \tag{78}$$

This function can be written as

$$B_0(p^2, m_1^2, m_2^2) = \frac{1}{\hat{\epsilon}} - \int_0^1 dx \ln \frac{(1-x)\,m_1^2 + x\,m_2^2 - x(1-x)\,p^2}{Q^2} \ . \tag{79}$$

Such Feynman parameter integral forms are especially useful in analytically evaluating the Passarino-Veltman functions in special cases, such as when one of its arguments is zero. The explicit formula for B_0 in the general case can be found in Ref. [6].

The vector two-point function is defined as

$$Q^{4-n} \int \frac{d^n q}{(2\pi)^n} \frac{q^\mu}{[q^2 - m_1^2 + i\varepsilon]\,[(q-p)^2 - m_2^2 + i\varepsilon]} \equiv \frac{i}{16\pi^2} B_1(p^2, m_1^2, m_2^2) p^\mu \ . \tag{80}$$

B_1 has the Feynman parameter integral representation

$$B_1(p^2, m_1^2, m_2^2) = \frac{1}{2\hat{\epsilon}} - \int_0^1 dx\, x \ln \frac{(1-x)\,m_1^2 + x\,m_2^2 - x(1-x)\,p^2}{Q^2} \ . \tag{81}$$

The tensor two-point functions are defined as

$$\begin{aligned} & Q^{4-n} \int \frac{d^n q}{(2\pi)^n} \frac{q^\mu q^\nu}{[q^2 - m_1^2 + i\varepsilon]\,[(q-p)^2 - m_2^2 + i\varepsilon]} \\ & \quad = \frac{i}{16\pi^2} \left[B_{21}(p^2, m_1^2, m_2^2) p^\mu p^\nu + B_{22}(p^2, m_1^2, m_2^2) g^{\mu\nu} \right] \ . \end{aligned} \tag{82}$$

The vector and tensor two-point functions can be written in terms of the scalar functions A_0 and B_0 as

$$\begin{aligned} & B_1(p^2, m_1^2, m_2^2) \\ & \quad = \frac{1}{2p^2} \left\{ A_0(m_2^2) - A_0(m_1^2) + (p^2 + m_1^2 - m_2^2) B_0(p^2, m_1^2, m_2^2) \right\} \ , \end{aligned} \tag{83}$$

$$\begin{aligned} & B_{21}(p^2, m_1^2, m_2^2) \\ & \quad = \frac{1}{3p^2} \left\{ 2A_0(m_2^2) - A_0(m_1^2) + \left(p^2 + \frac{m_1^2 - 5m_2^2}{4} \right) B_0(p^2, m_1^2, m_2^2) \right. \\ & \quad \left. - \frac{m_2^2 - m_1^2}{p^2} \left[A_0(m_2^2) - A_0(m_1^2) + \left(\frac{3}{4} p^2 + m_1^2 - m_2^2 \right) B_0(p^2, m_1^2, m_2^2) \right] \right. \end{aligned} \tag{84}$$

$$-\frac{1}{2}\left(m_1^2+m_2^2-\frac{1}{3}p^2\right)\Bigg\}\ ,$$

$$B_{22}(p^2,m_1^2,m_2^2) \tag{85}$$
$$=\frac{1}{6}\Bigg\{\frac{1}{2}\left(A_0(m_1^2)+A_0(m_2^2)\right)+\left(m_1^2+m_2^2-\frac{1}{2}p^2\right)B_0(p^2,m_1^2,m_2^2)$$
$$+\frac{m_2^2-m_1^2}{2p^2}\Big[A_0(m_2^2)-A_0(m_1^2)-(m_2^2-m_1^2)B_0(p^2,m_1^2,m_2^2)\Big]$$
$$+m_1^2+m_2^2-\frac{1}{3}p^2\Bigg\}\ .$$

The three-point scalar functions depend on the three external momenta, and the masses of the three internal lines. Hence, the functions take as arguments $(k^2,p_1^2,p_2^2,m_1^2,m_2^2,m_3^2)$, where m_1 is the mass of the internal line between k and p_1, and m_2 is the mass of the line between p_1 and p_2. The scalar function is

$$Q^{4-n}\int\frac{d^nq}{(2\pi)^n}\frac{1}{[q^2-m_1^2+i\varepsilon]\,[(q-p_1)^2-m_2^2+i\varepsilon]\,[(q-p_1-p_2)^2-m_3^2+i\varepsilon]}$$
$$\equiv\frac{i}{16\pi^2}C_0\ . \tag{86}$$

The vector and tensor three-point function integrals are defined as

$$Q^{4-n}\int\frac{d^nq}{(2\pi)^n}\frac{q^\mu}{[q^2-m_1^2+i\varepsilon]\,[(q-p_1)^2-m_2^2+i\varepsilon]\,[(q-p_1-p_2)^2-m_3^2+i\varepsilon]}$$
$$\equiv\frac{i}{16\pi^2}\Big[C_{11}\,p_1^\mu+C_{12}\,p_2^\mu\Big]\ , \tag{87}$$

and

$$Q^{4-n}\int\frac{d^nq}{(2\pi)^n}\frac{q^\mu q^\nu}{[q^2-m_1^2+i\varepsilon]\,[(q-p_1)^2-m_2^2+i\varepsilon]\,[(q-p_1-p_2)^2-m_3^2+i\varepsilon]}$$
$$\equiv\frac{i}{16\pi^2}\Big[C_{21}\,p_1^\mu p_1^\nu+C_{22}\,p_2^\mu p_2^\nu+C_{23}\,\{p_1^\mu p_2^\nu+p_2^\mu p_1^\nu\}+C_{24}\,g^{\mu\nu}\Big]\ . \tag{88}$$

Analytic formulae for the C-functions can be found in Ref. [14]. The evaluation of these functions can involve large cancellations, so much care should be exercised in implementing algorithms. A `FORTRAN` package, `FF`, is available which accurately evaluates these integrals, and more [15].

It is much more important to be familiar with the definitions and general properties of these functions than to be concerned with the general formula for them. For example, notice the general feature that the residue of the $1/\hat{\epsilon}$ pole of each function is the same as the coefficient of $\ln Q^2$. In the calculation of a physical quantity (such as the W-boson mass) the $1/\hat{\epsilon}$ divergences cancel out. This cancellation exactly corresponds to the cancellation of the renormalization scale dependence.

It is useful to note the behavior of the Passarino-Veltman functions in the limit that one of the arguments is large. Looking at B_0, for example, we can see from Eq. (79) that in the limit $M \gg m$,

$$B_0(M^2, m^2, m^2) = \frac{1}{\hat{\epsilon}} - \ln\frac{M^2}{Q^2} + \text{ const } + \mathcal{O}\left(\frac{m^2}{M^2}\right) . \tag{89}$$

This form is true for any ordering of arguments M and m. $2B_1$ also has the same form.

Example: SUSY-QCD corrections to the top quark mass

Given these definitions it is easy to evaluate one-loop Feynman diagrams. For example, consider the QCD correction to the top quark mass. The color factor is

$$T^a_{ik}T^a_{kj} = C_2(R)\delta_{ij} = \frac{N_c^2 - 1}{2N_c}\delta_{ij} = \frac{4}{3}\delta_{ij} \ , \tag{90}$$

and the diagram is evaluated as

$$\begin{aligned} i\Sigma(\not{p}) &= -\left(\frac{4g_3^2}{3}\right) Q^{4-n} \int \frac{d^nq}{(2\pi)^n} \frac{\gamma_\mu(\not{q} + m_t)\gamma^\mu}{[(q^2 - m_t^2) + i\varepsilon]\,[(q-p)^2 + i\varepsilon]} \\ &= -\frac{i}{16\pi^2}\left(\frac{4g_3^2}{3}\right)\left[-2\not{p}B_1(p^2, m_t^2, 0) + 4m_t B_0(p^2, m_t^2, 0)\right] \ . \end{aligned} \tag{91}$$

From Eq. (29) we have $\delta m = \frac{1}{2}\left[\Sigma_L(m^2) + \Sigma_R(m^2)\right] m + \mathcal{R}e\ \Sigma_S(m^2)$, so the gluon contribution to δm_t is

$$\delta m_t = -\frac{g_3^2}{6\pi^2}\left[2B_0(m_t^2, m_t^2, 0) - B_1(m_t^2, m_t^2, 0)\right] m_t \ . \tag{92}$$

From the forms in Eqs. (79) and (81), we determine

$$B_0(m^2, m^2, 0) = \frac{1}{\hat{\epsilon}} + \ln\frac{Q^2}{m^2} + 2 \ , \tag{93}$$

$$B_1(m^2, m^2, 0) = \frac{1}{2\hat{\epsilon}} + \frac{1}{2}\ln\frac{Q^2}{m^2} + \frac{3}{2} \ . \tag{94}$$

Hence, the gluon contribution to the top quark mass in $\overline{\rm DR}$ renormalization is

$$\delta\hat{m}_t = -\frac{\alpha_s}{3\pi}\left[3\ln\left(\frac{Q^2}{m_t^2}\right)+5\right]m_t \ . \tag{95}$$

The top quark mass is an input parameter, and as such its counterterm is renormalization scale and renormalization scheme *dependent*. The combination of counterterms and proper functions in the prediction of a physical quantity is renormalization scale and renormalization scheme *independent*.

As a second example, consider the squark/gluino contribution to the top quark self-energy. If we ignore squark mixing, the left-handed top squark contributes

$$i\Sigma(\not{p}) = \frac{8g_3^2}{3}Q^{4-n}\int\frac{d^nq}{(2\pi)^n}\frac{P_R(\not{q}+m_{\tilde{g}})P_L}{\left[q^2-m_{\tilde{g}}^2+i\varepsilon\right]\left[(q-p)^2-m_{\tilde{t}_L}^2+i\varepsilon\right]} \tag{96}$$

$$= \frac{8g_3^2}{3}\left(\frac{i}{16\pi^2}\right)B_1(p^2,m_{\tilde{g}}^2,m_{\tilde{t}_L}^2)\,\not{p}\,P_L \ , \tag{97}$$

so

$$\Sigma_L(p^2) = \frac{g_3^2}{6\pi^2}B_1(p^2,m_{\tilde{g}}^2,m_{\tilde{t}_L}^2) \ . \tag{98}$$

Including the right-handed top squark contribution, we find the correction to δm_t,

$$\delta m_t = \frac{\alpha_s}{3\pi}\mathcal{R}e\,\left(B_1(m_t^2,m_{\tilde{g}}^2,m_{\tilde{t}_L}^2)+B_1(m_t^2,m_{\tilde{g}}^2,m_{\tilde{t}_R}^2)\right)m_t \ . \tag{99}$$

From Eq. (81), we see that in the limit $m_{\tilde{t}} \gg m_{\tilde{g}},\ m_t$, the function B_1 becomes

$$B_1(m_t^2,m_{\tilde{g}}^2,m_{\tilde{t}}^2) = \frac{1}{2\hat{\epsilon}}+\frac{1}{2}\ln\left(\frac{Q^2}{m_{\tilde{t}}^2}\right)+\frac{1}{4}+\mathcal{O}\left(\frac{m_{\tilde{g}}^2,m_t^2}{m_{\tilde{t}}^2}\right) \tag{100}$$

After $\overline{\rm DR}$ renormalization the full SUSY-QCD top quark mass correction is then, in the limit $m_{\tilde{t}} = m_{\tilde{t}_L} = m_{\tilde{t}_R} \gg m_t,\ m_{\tilde{g}}$,

$$\delta\hat{m}_t = \frac{\alpha_s}{3\pi}\left[-3\ln\left(\frac{Q^2}{m_t^2}\right)-5+\ln\left(\frac{Q^2}{m_{\tilde{t}}^2}\right)+\frac{1}{2}+\mathcal{O}\left(\frac{m_{\tilde{g}}^2,m_t^2}{m_{\tilde{t}}^2}\right)\right]m_t \ . \tag{101}$$

The pole mass is related to the running $\overline{\rm DR}$ mass as

$$m_t = \hat{m}_t(Q) - \delta\hat{m}_t \ . \tag{102}$$

3.2 Threshold corrections and the RGE

We have just calculated the SUSY-QCD correction to the top quark mass. The top quark mass is an input parameter in the standard model. It is not a prediction. Hence, the correction is Q-dependent, and in order to obtain a finite result in four dimensions one must prescribe a renormalization procedure. We used $\overline{\rm DR}$ renormalization.

We see that the correction (101) involves logarithms. If a logarithmic correction is large the validity of perturbation theory may be threatened, as the expansion parameter in the perturbation series becomes $(\alpha/\pi)\log(M/m)$. Fortunately, these logarithmic corrections can be resummed to all orders in perturbation theory. The renormalization group equation serves this purpose.

The renormalization group equation for the top quark mass can be derived from Eq. (101). Since the top quark pole mass is scale independent, we have

$$\frac{d\,m_t}{d\ln Q^2} = 0 \quad \Longrightarrow \quad \frac{d\,\hat{m}_t}{d\ln Q^2} = \frac{d\,\delta\hat{m}_t}{d\ln Q^2} = -\frac{1}{16\pi^2}\left(\frac{8}{3}\hat{g}_3^2(Q) + \cdots\right)\hat{m}_t(Q) \tag{103}$$

where the dots indicate gauge and Yukawa coupling contributions from the other (non-QCD) loops. The RGE involves the Q-dependent $\overline{\rm DR}$ top quark mass and the Q-dependent $\overline{\rm DR}$ gauge and Yukawa couplings. There are RG equations for these couplings as well, and together they form a set of coupled differential equations. There is no closed form solution to these equations, but it is easy to solve them numerically.

We will now examine how the logarithmic and the non-logarithmic corrections in Eq. (101) relate to the RGE. For simplicity we will set $m_{\tilde{g}} = m_t$. If $m_{\tilde{t}} \gg m_t$, there is no single scale where the correction (101) is small. At the scale m_t, the squark loop contribution is proportional to $\ln(m_{\tilde{t}}/m_t)$. At the scale $Q = m_{\tilde{t}}$ the gluon loop contribution involves the same large logarithm. The RGE resums the large logarithms. Suppose we know the top quark pole mass, and we want to determine the top quark running mass at scales above the top squark mass. To resum the logs in Eq. (101) we first apply the gluon correction at the scale m_t. Notice there is no logarithm at this scale, so

$$\hat{m}_t(m_t) = \left(1 - \frac{5\hat{\alpha}_s(m_t)}{3\pi}\right) m_t \ . \tag{104}$$

Now we solve the RGE to evaluate this running mass at the top squark scale. The full RGE for the top quark mass involves all the gauge and Yukawa couplings and must be solved numerically. Here we will neglect all but the strong coupling so that we can solve it directly. In the effective theory below the top

squark mass scale, only the gluon contributes to the m_t RGE. Hence, from Eq. (101), the relevant RGE is

$$\frac{d\,\hat{m}_t(t)}{dt} = -\frac{\hat{g}_3^2(t)}{4\pi^2}\hat{m}_t(t) \ , \tag{105}$$

where $t = \ln Q^2$. At one-loop order, the strong coupling RGE is

$$\frac{d\,\hat{g}_3(t)}{dt} = \frac{b_3}{16\pi^2}\hat{g}_3^3(t) \ . \tag{106}$$

In the regime below the squark mass scale, but above the gluino mass scale, we have $b_3 = 5$. The solution to this equation is

$$\hat{g}_3^{-2}(Q_2) = \hat{g}_3^{-2}(Q_1) - \frac{b_3}{8\pi^2}\ln\left(\frac{Q_2^2}{Q_1^2}\right) \ . \tag{107}$$

We can plug this into Eq. (105) to solve for $\hat{m}_t(t)$. We find

$$\hat{m}_t(Q) = \hat{m}_t(m_t)\left(\frac{\hat{\alpha}_s(m_t)}{\hat{\alpha}_s(Q)}\right)^{\frac{2}{b_3}} \ . \tag{108}$$

This expression resums the logarithmic gluonic corrections to the top quark mass. It is good at any scale between the top quark mass and the top squark mass. To determine the running top quark mass above the squark mass scale, we must include the top squark loop correction. To avoid a large logarithm, which could spoil perturbation theory, we apply the top squark correction at the top squark mass scale. At this scale the logarithm in the top squark correction vanishes. The running top quark mass just above the top squark mass scale is

$$\hat{m}_t(m_{\tilde{t}}) = \left[\left(1 - \frac{5\hat{\alpha}_s(m_t)}{3\pi}\right)\left(\frac{\hat{\alpha}_s(m_t)}{\hat{\alpha}_s(m_{\tilde{t}})}\right)^{\frac{2}{5}} + \frac{\hat{\alpha}_s(m_{\tilde{t}})}{3\pi}\left(\frac{1}{2} + \mathcal{O}\left(\frac{m_t^2}{m_{\tilde{t}}^2}\right)\right)\right] m_t \ . \tag{109}$$

From this point we can run the top quark mass to higher scales by solving the full MSSM RGE. Notice that above the top squark mass scale both the top quark mass RGE and the strong coupling RGE change, due to the squark contributions.

This example illustrates how to use the RGE to resum large logarithms. It also demonstrates the interplay between the RGE and the logarithmic and non-logarithmic parts of the threshold corrections.

4 Z-pole precision data and calculation of the effective couplings

We have renormalized the electroweak sector of the standard model. Since the MSSM has the same gauge symmetry as the standard model, this renormalization also applies in the MSSM. Consider the $\overline{\rm DR}$ weak mixing angle, for example. We replace the bare parameters with the renormalized ones plus a shift

$$s_b^2 c_b^2 = \frac{\pi\alpha_b}{\sqrt{2}\,G_{\mu_b} M_{Z_b}^2} \quad \Rightarrow \quad \hat{s}^2\hat{c}^2 = \frac{\pi\alpha}{\sqrt{2}\,(G_\mu + \delta\hat{G}_\mu)(M_Z^2 + \delta\hat{M}_Z^2)(1-\Delta\hat{\alpha})} \tag{110}$$

to obtain

$$\hat{s}^2\hat{c}^2 = \frac{\pi\alpha}{\sqrt{2}\,G_\mu M_Z^2}\,\left[\frac{1}{1-\Delta\hat{r}_Z}\right]\,, \tag{111}$$

$$\begin{aligned}\Delta\hat{r}_Z &= \Delta\hat{\alpha} - \frac{\delta\hat{M}_Z^2}{M_Z^2} - \frac{\delta\hat{G}_\mu}{G_\mu} \\ &= \hat{\Pi}^{T\prime}_{\gamma\gamma}(0) + 2\,\frac{s}{c}\,\frac{\hat{\Pi}^T_{\gamma Z}(0)}{M_Z^2} - \mathcal{R}e\,\frac{\hat{\Pi}^T_{ZZ}(M_Z^2)}{M_Z^2} + \frac{\hat{\Pi}^T_{WW}(0)}{M_W^2} + \hat{\delta}_{VB}\,.\end{aligned} \tag{112}$$

The first 4 terms in the last expression for $\Delta\hat{r}_Z$ form the oblique part of the correction, *i.e.* the gauge boson self-energy contribution. The last part, $\hat{\delta}_{VB}$, is the non-oblique part of the correction. In the MSSM both the oblique and non-oblique terms receive superpartner loop contributions.

Applying this renormalization leads to predictions for observables in the MSSM which can be compared with experiment. Such comparisons can show which regions of supersymmetry parameter space are favored, and show that certain regions are inconsistent with the data.

We already determined the prediction for the W-boson mass. We shall now derive expressions for other precision observables. Most of the precision data is due to measurements of Z-boson production and decay. We write the effective Z-boson–fermion–anti-fermion vertex as $-i\gamma_\mu(g_v^{\rm eff} - g_a^{\rm eff}\gamma_5) = -i(g_L^{\rm eff}\,P_L + g_R^{\rm eff}\,P_R)$. The effective couplings depend on the effective charge and the effective weak mixing angle as

$$\begin{aligned} g_v^{\rm eff} &= \tfrac{e^{\rm eff}}{2s^{\rm eff}c^{\rm eff}}\,(T_3 - 2Q(s^{\rm eff})^2), & g_L^{\rm eff} &= \tfrac{e^{\rm eff}}{s^{\rm eff}c^{\rm eff}}\,(T_3 - Q(s^{\rm eff})^2)\,, \\ g_a^{\rm eff} &= \tfrac{e^{\rm eff}}{2s^{\rm eff}c^{\rm eff}}\,T_3\,, & g_R^{\rm eff} &= -\tfrac{e^{\rm eff}s^{\rm eff}}{c^{\rm eff}}\,Q\,. \end{aligned} \tag{113}$$

We will derive expressions for $(s^{\rm eff})^2$ and $(e^{\rm eff}/s^{\rm eff}c^{\rm eff})$. First we introduce related observables.

The fermion left-right asymmetry is

$$A_f = \frac{(g_{Lf}^{\rm eff})^2 - (g_{Rf}^{\rm eff})^2}{(g_{Lf}^{\rm eff})^2 + (g_{Rf}^{\rm eff})^2} = \frac{2 g_{vf}^{\rm eff} g_{af}^{\rm eff}}{(g_{vf}^{\rm eff})^2 + (g_{af}^{\rm eff})^2} \ . \tag{114}$$

Note that this asymmetry is independent of the electric charge. Hence a measurement of A_f is just a measurement of the effective weak mixing angle, $(s_f^{\rm eff})^2 = \sin^2\theta_f^{\rm eff}$. In principle, each fermion has its own weak mixing angle in its coupling to the Z. Each fermion also couples with its own strength, which is measured by the partial widths, Γ_f. The partial widths are proportional to $(g_{vf}^{\rm eff})^2 + (g_{af}^{\rm eff})^2$.

The polarized electron beam allows SLC to measure the initial and final state asymmetries independently. The left-right asymmetry

$$A_{LR} = \frac{\sigma_L - \sigma_R}{\sigma_L + \sigma_R} = A_e \tag{115}$$

is independent of the final state couplings. The polarized forward-backward asymmetry, on the other hand, is independent of the initial state couplings,

$$A_{FB}^{\rm pol} = \frac{1}{P}\ \frac{(N_{P,F} - N_{-P,F}) - (N_{P,B} - N_{-P,B})}{(N_{P,F} - N_{-P,F}) + (N_{P,B} - N_{-P,B})} = \frac{3}{4}\, A_f \ . \tag{116}$$

P is the polarization defined by $P = (P_{e^-} - P_{e^+})/(1 - P_{e^-}P_{e^+})$ and $N_{P,F}$ ($N_{P,B}$) is the number of fermions produced in the forward (backward) direction. SLC measures A_f for $f = e, \mu, \tau, b, c$. SLC also measures the heavy quark observables $R_{b,c} = \Gamma_{b,c}/\Gamma_{\rm had}$ and $A_{b,c}^{FB}$.

At LEP the beams are unpolarized. Hence, when the forward-backward asymmetry is measured,

$$A_f^{FB} = \frac{\sigma_F - \sigma_B}{\sigma_F + \sigma_B} = \frac{3}{4}\, A_e A_f \ , \tag{117}$$

a combination of the initial and final state effective weak mixing angles is determined. There are other means to measure A_e independently at LEP. For example, a measurement of A_e^{FB} determines A_e. Also, they can extract both A_e and A_τ from the τ-polarization measurement,

$$P_\tau(\cos\theta) = -\frac{A_\tau + A_e f(\cos\theta)}{1 + A_\tau A_e f(\cos\theta)} \ , \qquad f(x) = \frac{2x}{1+x^2} \ . \tag{118}$$

Of course the various partial widths are also measured at LEP. The measurements include

$$A_f^{FB}, \ f = e, \mu, \tau, b, c \ , \tag{119}$$

$$A_{e,\tau} \ , \tag{120}$$

$$\Gamma_Z \propto \sum_f (g_{v_f}^{\rm eff})^2 + (g_{a_f}^{\rm eff})^2 \ , \tag{121}$$

$$\sigma_{\rm had} = \frac{12\pi}{M_Z^2} \ \frac{\Gamma_e \Gamma_{\rm had}}{\Gamma_Z^2} \ , \tag{122}$$

$$R_\ell = \frac{\Gamma_{\rm had}}{\Gamma_\ell} \ , \quad \ell = e, \mu, \tau \ , \tag{123}$$

$$R_{b,c} = \frac{\Gamma_{b,c}}{\Gamma_{\rm had}} \ , \tag{124}$$

as well as $\sin^2 \theta_e^{\rm eff}$ from the forward-backward charge asymmetry $\langle Q_{FB} \rangle$.

The LEP and SLC collaborations do not present their results in a model-independent fashion. In extracting the values of observables from the data they assume the gauge structure of the standard model. That is, they assume the process $e^+e^- \to f\overline{f}$ is mediated by standard model processes: s and t channel γ and Z exchange, and box diagrams involving γ, W and Z exchange. The diagrams involving the photon (the s- and t-channel exchange, the photonic box diagrams, and the $\gamma - Z$ interference) are taken into account by the experimentalists. In other words, these contributions are subtracted from the data. The photonic corrections are small. On the Z-pole they are suppressed by a factor Γ_Z/M_Z. The genuine electroweak box diagrams are also suppressed, and can be neglected. In the SM and in the MSSM, the remaining processes only involve the Z-fermion-antifermion vertex. Thus, by subtracting the photon contributions the Z-vertices are isolated. In this way measurements of the coupling of the Z to $f\overline{f}$ are quoted. It is good to keep in mind the model dependence of the quoted results. If other particles mediate the $e^+e^- \to f\overline{f}$ process, the quoted values of the effective Z-couplings are incorrect. In the MSSM (with R-parity), however, the only new processes which mediate $e^+e^- \to f\overline{f}$ are superpartner box diagrams. On the Z-pole these contributions are negligible. Hence, the effective coupling analysis is ideally suited to the MSSM. One needs only to compute the supersymmetric corrections to the effective couplings, and compare to the quoted values.

Virtual loops involving superpartners change the effective $Zf\overline{f}$ couplings. This is the only relevant supersymmetric correction in Z-pole data. We now derive the form of the Z-vertex corrections. We apply the same renormalization procedure as in the Sec. 2. The bare Lagrangian is of the form

$$\mathcal{L} = -\overline{\psi}_b \gamma_\mu (g_{v_b} - g_{a_b}\gamma_5) \, \psi_b Z_b^\mu - e_b Q \ \overline{\psi}_b \gamma_\mu \psi_b A_b^\mu \ . \tag{125}$$

As usual, we apply wave-function renormalization and replace the bare couplings by the renormalized couplings plus the counterterms,

$$\mathcal{L} = -\overline{\psi}\gamma_\mu \Big[(g_v + \delta g_v)(Z_v - Z_a\gamma_5) - (g_a + \delta g_a)(Z_v - Z_a\gamma_5)\gamma_5 \Big] \psi \tag{126}$$
$$\times \Big[Z_{ZZ}^{\frac{1}{2}} Z^\mu + Z_{Z\gamma}^{\frac{1}{2}} A^\mu \Big] - (e + \delta_e) Q\, \overline{\psi}\gamma_\mu (Z_v - Z_a\gamma_5)\psi \Big[Z_{\gamma\gamma}^{\frac{1}{2}} A^\mu + Z_{\gamma Z}^{\frac{1}{2}} Z^\mu \Big] \ .$$

The Z-vertex may be read off, and at one-loop order we simply add the proper three point function $\delta\Lambda(k^2, p_1^2, p_2^2)$ to obtain the renormalized vertex (we neglect the magnetic moment contribution)

$$i\Gamma_\mu(k^2, p_1^2, p_2^2) = \tag{127}$$
$$-i\gamma_\mu \Bigg[g_v \left(Z_v + \frac{g_a}{g_v} Z_a + \frac{\delta g_v}{g_v} + \frac{1}{2}\, \delta Z_{ZZ} + \frac{eQ}{g_v}\, Z_{\gamma Z}^{\frac{1}{2}} + \frac{\delta\Lambda_v(k^2, p_1^2, p_2^2)}{g_v} \right)$$
$$- g_a \left(Z_v + \frac{g_v}{g_a} Z_a + \frac{\delta g_a}{g_a} + \frac{1}{2}\, \delta Z_{ZZ} + \frac{\delta\Lambda_a(k^2, p_1^2, p_2^2)}{g_a} \right) \gamma_5 \Bigg] \ .$$

At this point we can apply $\overline{\rm DR}$ renormalization to the couplings. The counterterms δg_v and δg_a are then purely 'infinite' (*i.e.* proportional to $1/\hat{\epsilon} = 1/\epsilon + \ln 4\pi - \gamma_E$) and are cancelled by the 'infinite' parts of the other terms. The $\overline{\rm DR}$ couplings $\hat{g}_v$ and $\hat{g}_a$ are in tree-level relationship with $\hat{e}$ and $\hat{s}$, which we have renormalized already. On the Z-pole the effective axial coupling squared is

$$(g_a^{\rm eff})^2 = \frac{\hat{e}^2}{4\hat{s}^2\hat{c}^2}\, T_3^2 \left(1 - \Big[\hat{\Sigma}_L(0) + \hat{\Sigma}_R(0) \Big] - \frac{g_v}{g_a} \Big[\hat{\Sigma}_L(0) - \hat{\Sigma}_R(0) \Big] \right.$$
$$\left. - \mathcal{R}e\ \hat{\Pi}_{ZZ}^{T\prime}(M_Z^2) + 2\, \frac{\delta\hat{\Lambda}_a(M_Z^2, 0, 0)}{g_a} \right) , \tag{128}$$

where we have neglected the fermion mass. From Eq. (69) we have

$$\frac{\hat{e}^2}{4\hat{s}^2\hat{c}^2} = \sqrt{2}\, G_\mu M_Z^2 \left(1 + \frac{\delta\hat{M}_Z^2}{M_Z^2} + \frac{\delta\hat{G}_\mu}{G_\mu} \right)$$
$$= \sqrt{2}\, G_\mu M_Z^2 \left(1 + \mathcal{R}e\ \frac{\hat{\Pi}_{ZZ}^T(M_Z^2)}{M_Z^2} - \frac{\hat{\Pi}_{WW}^T(0)}{M_W^2} - \hat{\delta}_{VB} \right) \tag{129}$$

so

$$(g_a^{\rm eff})^2 = \frac{\sqrt{2}\,G_\mu M_Z^2}{4}\left(1 + \mathcal{R}e\;\frac{\hat\Pi_{ZZ}^T(M_Z^2)}{M_Z^2} - \mathcal{R}e\;\hat\Pi_{ZZ}^{T\prime}(M_Z^2) - \frac{\hat\Pi_{WW}^T(0)}{M_W^2}\right. \tag{130}$$

$$\left. - \left[\hat\Sigma_L(0) + \hat\Sigma_R(0)\right] - \frac{g_v}{g_a}\;\left[\hat\Sigma_L(0) - \hat\Sigma_R(0)\right] + 2\;\frac{\delta\hat\Lambda_a(M_Z^2,0,0)}{g_a} - \hat\delta_{VB}\right)\,.$$

$g_a^{\rm eff}$ determines the strength of the effective couplings. The correction to the effective mixing angle is determined by $g_v^{\rm eff}/g_a^{\rm eff}$,

$$g_v^{\rm eff} = \frac{g_a^{\rm eff}}{T_3}\;(T_3 - 2Q\,s^2_{\rm eff}) \qquad \Rightarrow \qquad s^2_{\rm eff} = \frac{1}{4|Q|}\;\left(1 - \frac{g_v^{\rm eff}}{g_a^{\rm eff}}\right)\;. \tag{131}$$

We define $\hat\kappa$ to be the ratio of $s^2_{\rm eff}$ to $\hat s^2$. The correction to $\hat\kappa$ is given by

$$\Delta\hat\kappa = \left(\frac{1}{4|Q|^2 s^2} - 1\right)\;\left(\frac{\Delta\hat g_a}{g_a} - \frac{\Delta\hat g_v}{g_v}\right)\;, \tag{132}$$

where $\Delta\hat g_a/g_a$ and $\Delta\hat g_v/g_v$ are the corrections inside the parentheses in Eq. (127), in the $\overline{\rm DR}$ scheme. Note the common Z and vector fermion wave-function renormalizations cancel out, leaving

$$\Delta\hat\kappa = \left(\frac{1}{4|Q|^2 s^2} - 1\right)\left[\frac{eQ}{g_v}\;\frac{\hat\Pi_{\gamma Z}^T(M_Z^2)}{M_Z^2} + \frac{g_v^2 - g_a^2}{2g_v g_a}\;\left[\hat\Sigma_L(0) - \hat\Sigma_R(0)\right]\right.$$
$$\left. + \frac{\delta\hat\Lambda_a(M_Z^2,0,0)}{g_a} - \frac{\delta\hat\Lambda_v(M_Z^2,0,0)}{g_v}\right] \tag{133}$$

$$= \frac{c}{s}\;\frac{\hat\Pi_{\gamma Z}^T(M_Z^2)}{M_Z^2} + \left(\frac{1}{4|Q|^2 s^2} - 1\right)\;\left[\frac{g_v^2 - g_a^2}{2g_v g_a}\;\left[\hat\Sigma_L(0) - \hat\Sigma_R(0)\right]\right.$$
$$\left. + \frac{\delta\hat\Lambda_a(M_Z^2,0,0)}{g_a} - \frac{\delta\hat\Lambda_v(M_Z^2,0,0)}{g_v}\right]\,.$$

We obtain the effective weak mixing angle by multiplying $\hat s^2$ from Eq. (69) with $\hat\kappa = 1 + \Delta\hat\kappa$. The most important supersymmetric contributions to $\delta\hat\Lambda_v$ and $\delta\hat\Lambda_a$ are listed for the $Zb\,\overline{b}$ coupling in Ref. [16]. Generalizing to the other fermion couplings is straightforward.

5 Comparison of supersymmetric models and precision data: $\Delta\chi^2$ analysis

The effective Z-boson couplings we just derived allow us to calculate the following observables:

- Z-width

$$\Gamma_Z = \sum_f \Gamma_f = \sum_f \frac{\sqrt{2}\, G_\mu M_Z^3}{12\pi} \left[(g_{vf}^{\rm eff})^2 + (g_{af}^{\rm eff})^2 \right] \left[1 + \mathcal{O}(\alpha) \right]$$

- Ratio of hadronic to leptonic width

$$R_\ell = \frac{\Gamma_{\rm had}}{\Gamma_\ell}$$

- Peak hadronic cross section

$$\sigma_{\rm had} = \frac{12\pi}{M_Z^2} \frac{\Gamma_e \Gamma_{\rm had}}{\Gamma_Z^2}$$

- Ratio of heavy quark to hadronic width

$$R_{b,c} = \frac{\Gamma_{b,c}}{\Gamma_{\rm had}}$$

- Left-right asymmetry

$$\mathcal{A}_f = \frac{2 g_{vf}^{\rm eff} g_{af}^{\rm eff}}{(g_{vf}^{\rm eff})^2 + (g_{af}^{\rm eff})^2}$$

- Forward-backward asymmetry

$$A_f^{\rm FB} = \frac{3}{4} \mathcal{A}_e \mathcal{A}_f$$

- Forward-backward left-right asymmetry

$$A_{{\rm LR}\, f}^{\rm FB} = \mathcal{A}_f$$

- Effective weak mixing angle

$$\sin^2 \theta_f^{\rm eff} = \frac{1}{4|Q_f|} \left(1 - \frac{g_{vf}^{\rm eff}}{g_{af}^{\rm eff}} \right)$$

The calculation of the effective Z-boson couplings allows predictions for 20 precision observables. We can quantify the comparison of a theory with the measurements by forming a χ^2, which gives a measure of the goodness of the fit. We define the χ^2 below. The reliability of the results of this kind of test increases with the number of observables. Hence, we will consider the following 11 additional observables in the fit:

- **3 pole masses**

  The Z-mass measurement is now as precise as the G_μ measurement. We fix G_μ, but include M_Z in the fit since its error is correlated with other measurements. The combined W-mass measurements from CDF, D0, UA2, and LEP 2, give [17]

  $$M_W = 80.430 \pm 0.076 \text{ GeV}.$$

  The combination of results of all top decay channels at CDF and D0 gives [18]

  $$m_t = 175 \pm 5 \text{ GeV}.$$

  We take M_Z and m_t as inputs.

- **6 low energy observables**

  The weak charges of Tl and Cs have been measured in atomic parity violation experiments (APV), giving [19] $Q_W(^{205}\text{Tl}) = -114.77 \pm 1.23 \pm 3.44$, and $Q_W(^{133}\text{Cs}) = -72.11 \pm 0.27 \pm 0.89$. The deep inelastic scattering (DIS) experiments have produced a measurement of a linear combination of effective 4-Fermi operator coefficients [20], $\kappa(\text{DIS}) = 0.5805 \pm 0.0039$. The neutrino scattering experiments yield determinations of leptonic 4-Fermi operator coefficients [21], $g_V^{\nu e} = -0.041 \pm 0.015$ and $g_A^{\nu e} = -0.507 \pm 0.014$. Finally, the CLEO measurement [22] of $\text{B}(B \to X_s\gamma)$ yields the 90% confidence level interval $1 \times 10^{-4} < \text{B}(B \to X_s\gamma) < 4.2 \times 10^{-4}$. When an observable x is defined in a finite interval, there are arguments which suggest that a logistic transformation $y = \lg(x)$ should be performed, so that the new variable y is defined on the entire real axis. Including the transformed variable in the χ^2 results in a more Gaussian shaped distribution in that variable. Hence, we include $\lg(\text{B}(B \to X_s\gamma))$ in the χ^2. For a variable defined on (0,1) the logistic transformation is $\lg(x) = \ln(x/(1-x))$.

- **2 gauge couplings**

  We use the constraint $\Delta\alpha^{(5)}_{\text{had}} = 0.02817 \pm 0.00062$ [23]. We also include the constraint $\alpha_s(M_Z) = 0.118 \pm 0.003$, which we obtain by combining non-Z lineshape data [24].

These 11 observables, combined with the 20 effective coupling observables, give a total of 31 observables.

5.1 Global fit in the standard model

The measurements and experimental errors of the observables are listed in Table 1, along with the best fit values of the observables in the standard model. Input data are as of August, 1997. The fit is performed as follows. We construct the χ^2 by adding the square of the deviations,

$$\chi^2 = \sum_{i=1}^{31} \left(\frac{o_i^{\rm meas} - o_i^{\rm pred}}{\delta o_i} \right)^2 \quad ,$$

where $o_i^{\rm meas}$ and δo_i is the central value and error of the measurement of the i'th observable, and $o_i^{\rm pred}$ is the prediction. Four of the entries in Table 1 are inputs, so they do not have a prediction associated with them. In the corresponding term in the χ^2 in place of the predicted value we use the input value.

We then minimize the χ^2 function with respect to the inputs. In the standard model, these are M_Z, m_t, M_H, $\Delta\alpha^{(5)}_{\rm had}$, and $\alpha_s(M_Z)$. In the standard model the χ^2 analysis gives rise to pertinent information about the Higgs boson mass. We find a standard model central value of $M_H = 66$ GeV, and a 95% confidence level upper bound of about 330 GeV. The 68% and 95% confidence level contours are shown in Fig. 1 in the $(M_H,\ m_t)$ plane.

In the MSSM, the lightest Higgs boson is constrained by the form of the tree-level scalar potential to be below the Z-boson mass. Radiative corrections raise the upper bound to about 125 GeV, depending on the superpartner spectrum [25]. The lower bound on m_h in supersymmetric models is 78 GeV. We compare the range of m_h predicted in the MSSM with the best fit value in the SM in Fig. 1. We see that the range of values predicted in the MSSM falls within the 68% SM Higgs boson mass range.

5.2 Global fit in supersymmetric models

To discuss the global fit to the data in supersymmetry we have to specify the soft supersymmetry breaking Lagrangian. Since we don't know how supersymmetry is broken, we would, in the most general analysis, consider the most general soft breaking terms. However, this would lead to over one hundred parameters, with many complicated correlations needed among the parameters to ensure compliance with FCNC processes, rare decays, and so on. This is an

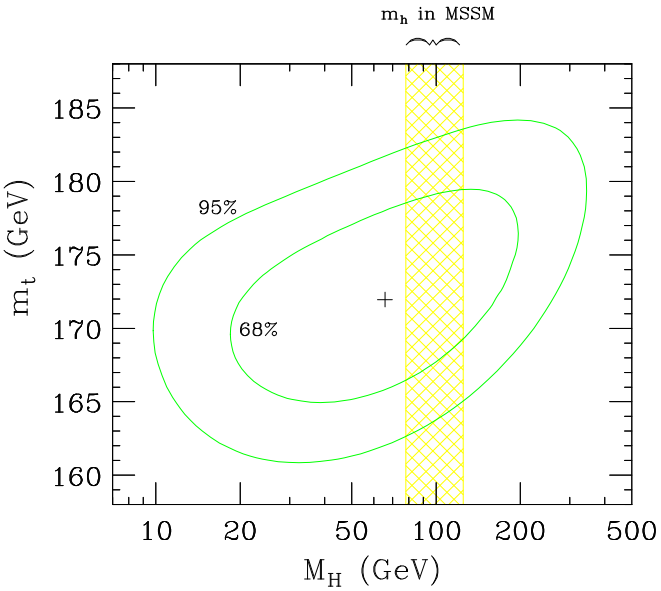

Figure 1: The 68 and 95% C.L. contours in the (m_t, M_H) plane in the standard model. The range of Higgs boson mass predicted in the MSSM is also shown.

intractable approach. Instead, we will consider specific high scale models, in which the soft Lagrangian takes a simple form. Besides reducing the parameter space to a manageable set, these models have the virtue of automatically satisfying the aforementioned constraints. We will consider two types of models, which are distinguished by how the supersymmetry breaking is communicated to the MSSM fields.

Supersymmetric models

In the canonical "minimal supergravity model" [26], supersymmetry breaking is parametrized by a universal F-term in a hidden sector. This supersymmetry breaking vev is communicated to the observable sector (*i.e.* the MSSM fields) by gravitational effects, giving rise to scalar masses, gaugino masses, and A-terms, all of order $F/M_P \simeq$ 100–1000 GeV. Since gravity is flavor blind, it is assumed that these mass parameters are universal. Hence, in this minimal model we take as inputs a universal scalar mass, M_0, a universal gaugino mass, $M_{1/2}$, and a universal trilinear scalar coupling, A_0. These inputs apply at the scale associated with the messenger particle, in this case the Planck scale.

However, for simplicity, and to avoid model dependence, we will take these inputs as valid at the scale where the U(1) and SU(2) gauge couplings unify, $M_{\rm GUT} \simeq 2 \times 10^{16}$ GeV.

In simple gauge-mediated models[27] supersymmetry is dynamically broken in a hidden sector. Interactions between the supersymmetry breaking sector and a standard model singlet, S, give rise to vevs in the lowest and F components of S. The singlet is coupled to so-called messenger fields, M and $\overline{M}$, through a superpotential coupling $SM\overline{M}$. Through this coupling the S vevs produce diagonal (supersymmetry conserving) and off-diagonal (supersymmetry breaking) entries in the (M, $\overline{M}$) mass matrix. The messenger fields are charged under the standard model gauge symmetries. Hence, through the usual gauge interactions, the supersymmetry breaking in the messenger fields is communicated to the MSSM fields. This gives rise to gaugino and scalar masses. The masses are proportional to the gauge couplings squared times the ratio of the F term of S to its scalar component, $\Lambda = F/S$. The masses also depend on the representation of the messenger fields. In order to maintain the near unification of couplings in the MSSM, we will consider complete SU(5) multiplets which do not affect gauge coupling unification at one loop. We'll consider a messenger sector made of n_5 $\mathbf{5}+\overline{\mathbf{5}}$ fields and n_{10} $\mathbf{10}+\overline{\mathbf{10}}$ fields. The gaugino masses and the scalar masses squared are proportional to the effective number of messenger $\mathbf{5}+\overline{\mathbf{5}}$ fields, $n_5^{\rm eff} = n_5 + 3n_{10}$. The trilinear A-terms are not generated at one-loop, so we set $A_0 = 0$ at the messenger scale. We will consider models with $n_5^{\rm eff} = 1$ (*i.e.* $n_5 = 1,\ n_{10} = 0$, the $\mathbf{5}+\overline{\mathbf{5}}$ model) and $n_5^{\rm eff} = 3$ (*i.e.* $n_5 = 0,\ n_{10} = 1$, the $\mathbf{10}+\overline{\mathbf{10}}$ model).

In both the gauge- and gravity-mediated models the spectrum of soft masses is given at some high scale (either $M_{\rm GUT}$ or the messenger scale M). In order to calculate the radiative corrections to the precision observables we need to determine the physical superpartner spectrum. We specify three steps to accomplish this. First, we need to run the soft mass parameters from the initial high scale down to the vicinity of the weak scale. As we describe below, an appropriate scale to stop the running is the squark mass scale. Second, we need to construct the weak scale mass matrices of the charginos, neutralinos, squarks, sleptons and Higgs bosons. These include the soft-breaking mass parameters and supersymmetry conserving terms proportional to the Higgsino mass parameter μ, the gauge boson masses and/or the fermion masses. We then determine the physical superpartner mass spectrum and mixing angles by finding the eigenvalues and eigenvectors of the mass matrices.

5.3 Electroweak symmetry breaking

In both the gravity- and gauge-mediated models we impose electroweak symmetry breaking[28]. Electroweak symmetry breaking occurs generically over the parameter space in both models. The RGEs of the Higgs boson soft masses include terms proportional to the Yukawa couplings. These terms drive the Higgs boson masses toward negative values. If $\tan\beta$ is not very large, the top quark Yukawa coupling is larger than the other Yukawa couplings, so the mass of the Higgs boson which couples to the top quark (H_2) is driven negative. This is exactly what is necessary to have electroweak symmetry breaking take place if $\tan\beta > 1$. In fact, because the bottom Yukawa coupling can become larger than the top Yukawa coupling at $\tan\beta \gtrsim 60$, the mass of the Higgs which couples to the bottom quark (H_1) can be driven too negative at large $\tan\beta$ and in this case electroweak symmetry breaking does not occur. This is why large $\tan\beta$ values are excluded in our analysis.

Imposing electroweak symmetry breaking allows us to compute the heavy Higgs boson mass and the Higgsino mass parameter μ[6]. Given the soft Higgs masses m_{H_1} and m_{H_2}, we can determine the CP-odd Higgs boson $\overline{\rm DR}$ mass $\hat{m}_A$, and the $\overline{\rm DR}$ Higgsino mass parameter μ,

$$\hat{m}_A^2 = \frac{\overline{m}_{H_2}^2 - \overline{m}_{H_1}^2}{\cos 2\beta} - \hat{M}_Z^2 \ , \tag{134}$$

$$\mu^2 = \frac{\tan^2\beta\, \overline{m}_{H_2}^2 - \overline{m}_{H_1}^2}{1-\tan^2\beta} - \frac{1}{2}\hat{M}_Z^2 \ . \tag{135}$$

$\hat{M}_Z$ is the $\overline{\rm DR}$ Z-boson mass ($\hat{M}_Z^2 = M_Z^2 + \mathcal{R}e\,\hat{\Pi}_{ZZ}^T(M_Z^2)$), and $\overline{m}_{H_i} = m_{H_i} - t_i/v_i$. The t_i are the tadpole diagram contributions. These corrections are necessary in order to ensure that we are at the minimum of the one-loop effective potential. They are the effective potential corrections in the diagrammatic approach. The contribution to t_i/v_i from a particle of mass m which couples to H_i is of the form $m^2\log(m/Q)$, where Q is the renormalization scale. Since the squarks are typically the heaviest particles, and because of the color and multiplicity factors, their contribution to the tadpole corrections usually dominates. The corrections to electroweak symmetry breaking can be applied most reliably at a scale Q where the tadpole corrections are minimized. This will generally be in the vicinity of the squark mass scale. This is why we stop the running of the soft parameters at the squark mass scale. At $Q = m_{\tilde{q}}$ the electroweak symmetry breaking conditions can be reliably computed. At scales far from $m_{\tilde{q}}$, large logarithms make perturbation theory less trustworthy.

We work in the convention that the gaugino masses are positive and μ can be either sign, so the sign of μ needs to be specified. To summarize, the

parameter space of the minimal supergravity model is

$$M_0,\ M_{1/2},\ A_0,\ \tan\beta,\ \mathrm{sgn}(\mu)\ , \tag{136}$$

and the gauge-mediated model parameter space is

$$M,\ \Lambda,\ \tan\beta,\ \mathrm{sgn}(\mu),\ n_5^{\mathrm{eff}}\ . \tag{137}$$

5.4 Results

We can now describe the results of the comparison of the predictions of these supersymmetric models with the precision observables. A more complete discussion can be found in Ref. [29]. Choosing a point in the parameter space of (136) or (137), we run down the soft mass parameters to the squark mass scale, and check for electroweak symmetry breaking. We then determine the physical superpartner masses and mixings. We check if any of the superpartner masses are below the current direct search limits. If so, we disregard that point, and pick a new point. If all the mass bounds are satisfied, we compute the supersymmetric correction to each observable, and add it to the standard model prediction. We can then evaluate χ^2 and minimize it with respect to the standard model input parameters, M_Z, m_t, $\Delta\alpha^{(5)}_{\mathrm{had}}$, and α_s. We have to iterate this process since the new values of M_Z, m_t, $\Delta\alpha^{(5)}_{\mathrm{had}}$, and α_s after minimization correspond to a different supersymmetric spectrum than the one found in the previous iteration.

The supersymmetric corrections have the following characteristics. For very large supersymmetric masses ($\tilde{m} \gg M_Z$) the supersymmetric corrections to the weak-scale observables decouple, and go to zero at least as fast as $M_Z/\tilde{m}$. In the large $\tilde{m}$ limit the predictions in any supersymmetric model will match those of the standard model, with the standard model Higgs mass equal to the light supersymmetric Higgs mass. As the superpartner masses become light, there can be relatively large corrections to the weak-scale observables, and in general these corrections will upset the near perfect standard model fit to the data shown in Table 1.

The oblique approximation

Before looking at the full one-loop results, it is instructive to consider an approximation. The full corrections can be divided up into two sets of corrections, those from gauge boson self-energies, and the vertex, wave-function and box diagram corrections. The first set, the gauge-boson self-energy corrections, are called the oblique corrections. They are universal in the sense that only

certain combinations of gauge boson self-energies appear in the corrections to every physical observable. In fact, in the lowest order of a derivative expansion, (where, for example, the derivative Π' is approximated by $[\Pi(M_Z^2) - \Pi(0)]/M_Z^2$) there are only three combinations of gauge boson self-energies which appear. We consider the combinations given by Peskin and Takeuchi [30], the S, T and U parameters. They are given by

$$S = \left[\cos^2\theta_W\,(F_{ZZ} - F_{\gamma\gamma}) - \frac{\cos\theta_W}{\sin\theta_W}\cos 2\theta_W\, F_{\gamma Z}\right] \times \frac{4\sin^2\theta_W}{\alpha}$$

$$T = \left[\frac{\Pi_{WW}(0)}{M_W^2} - \frac{\Pi_{ZZ}(0)}{M_Z^2} - 2\frac{\sin\theta_W}{\cos\theta_W}\frac{\Pi_{\gamma Z}(0)}{M_Z^2}\right] \times \frac{1}{\alpha}$$

$$U = \left[F_{WW} - \cos^2\theta_W F_{ZZ} - \sin^2\theta_W F_{\gamma\gamma} - \sin 2\theta_W F_{\gamma Z}\right] \times \frac{4\sin^2\theta_W}{\alpha}$$

where $F_{ij} = (\Pi_{ij}(M_j^2) - \Pi_{ij}(0))/M_j^2$ (except $F_{\gamma\gamma} = \Pi_{\gamma\gamma}(M_Z^2)/M_Z^2$). In the oblique approximation the non-oblique, process specific corrections (the vertex corrections, wave function renormalization, and box diagrams) are neglected. There is a simple argument why the oblique approximation is expected to be a good approximation. Every superpartner (except the gluino) couples to the electroweak gauge bosons, so every superpartner contributes to the oblique corrections. Hence, the oblique corrections are enhanced by large multiplicity factors. For example, there are 21 sfermion contributions. In contrast, only certain superpartners contribute to the non-oblique corrections. The non-oblique corrections are constrained by the specific flavor of the fermions on the external lines. Hence, the oblique corrections are expected in general to dominate over the non-oblique corrections.

The oblique approximation gives an encapsulated view of the supersymmetric corrections. Rather than looking at the corrections to 30 individual observables, one can simply compute the corrections to the three oblique parameters, and then consider which observables are sensitive to which oblique shifts. In Fig. 2 we show the full range of the supersymmetric corrections (found in a random scan of 50,000 points in parameters space) to the three oblique parameters in the supergravity model, versus the light chargino mass. We see that the corrections to T and U are always positive. The corrections to S and U are small, less than 0.1, while the corrections to T can be almost as large as 0.2.

These oblique shifts result in shifts in the prediction of each observable. We can ascertain the importance of the oblique corrections in the χ^2 by dividing the correction to each observable (due to the shift in each oblique parameter) by the experimental error. We show the range of the oblique corrections to various

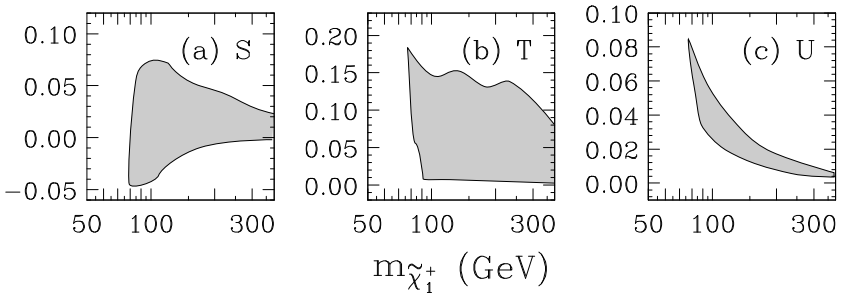

Figure 2: The range of the corrections to S, T and U in the supergravity model, vs. the light chargino mass.

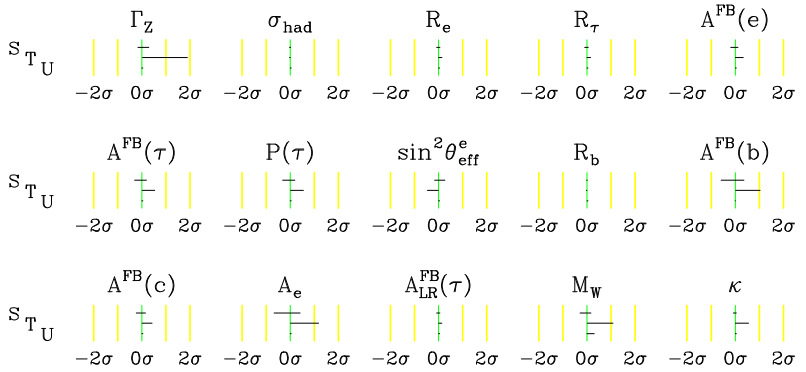

Figure 3: The range of the corrections to various observables due to the oblique corrections to S, T and U, in the supergravity model. The corrections are divided by the experimental error.

observables in the supergravity model in Fig. 3. We see that some observables, such as $\sigma_{\rm had}$, R_e and R_b receive negligible oblique corrections, while others, such as Γ_Z, A_e and M_W, receive substantial oblique corrections[e].

There are two types of corrections in going from the oblique approximation to the full one-loop corrections. Of course the process-specific corrections must be added (the vertex, wave function, and box diagram corrections). One also needs to correct for the full gauge boson self-energies. As we have seen, some of the gauge boson corrections enter as derivatives of the self-energies. In the oblique approximation the derivatives are approximated by a difference of self-

[e] We emphasize that the size of the corrections are measured against the current experimental error. Fig. 3 does not reflect the absolute size of the corrections.

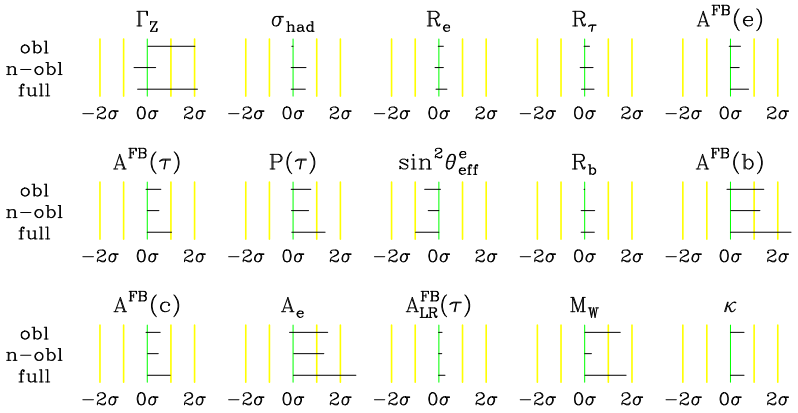

Figure 4: The range of the oblique (`obl`), non-oblique (`n-obl`) and full corrections to various observables in the supergravity model, divided by the experimental error. The non-oblique correction to κ is neglected.

energies. For the difference to be small, the particles in the loop should be much heavier than the gauge bosons. Hence, the oblique approximation should not work well when some superpartner masses are light, of order M_Z. This is just what we find. In Fig. 4 we compare the oblique, non-oblique and full corrections in the supergravity model. We show the maximum range of the corrections for various observables, in each case dividing by the experimental error. We see that for most of the observables the largest non-oblique corrections are about as large or larger than the largest oblique corrections. The region of parameter space with light superpartners has the largest corrections – and it is just in this region where the oblique approximation breaks down. Hence, when excluding regions of parameter space it is crucial to include the full one-loop corrections. We turn to the exclusion analysis next. We note that the oblique corrections to the low-energy observables $\kappa(\mathrm{DIS})$, $g_V^{\nu e}$, $g_A^{\nu e}$, $Q_W(\mathrm{Cs})$ and $Q_W(\mathrm{Tl})$ are all small relative to the experimental error. Hence, the non-oblique corrections are bound to be small as well. We treat these observables in the oblique approximation in the next section. For all other observables the full one-loop corrections are included.

Excluded regions of supersymmetric parameter space

We need to specify a criteria to exclude a point in supersymmetry parameter space based on the χ^2 test. We will use a criteria analogous to that used in determining the standard model Higgs boson mass limit. The 95% confidence

level limit on the Higgs boson mass corresponds to $\Delta\chi^2 = 3.84$. That is, if the difference between the minimum χ^2 value and the χ^2 value at a given Higgs boson mass is greater than 3.84, that value of the Higgs boson mass is excluded by the data with at least 95% confidence. We adopt this criteria directly to the supersymmetric models. In each model we randomly scan over 50,000 points in the parameter space, and find the minimum χ^2, $\chi^2_{\rm min}$. Then, at each point we compute $\Delta\chi^2 = \chi^2 - \chi^2_{\rm min}$. If $\Delta\chi^2$ is larger than 3.84 we consider this point in supersymmetry parameter space to be excluded by the data. We emphasize that at each point we minimize the χ^2 with respect to M_Z, m_t, $\Delta\alpha^{(5)}_{\rm had}$ and α_s.

We show the results in two dimensional subspaces. In each plot the dashed curve bounds the region of the parameter space which contains points which are excluded. The solid line bounds the region of parameter space containing points which are not excluded. Since we project a multidimensional parameter space onto two dimensions, there are regions which contain both excluded and unexcluded points in each figure. The regions bounded by the dashed curves which are outside the solid curves are absolutely excluded, independently of the values of other parameters. In the following we will focus on these absolutely excluded regions.

In each of the following figures, we show the results for the supergravity model, the $\mathbf{5} + \overline{\mathbf{5}}$ gauge-mediated model, and the $\mathbf{10} + \overline{\mathbf{10}}$ gauge-mediated model, in the three panes from left to right, respectively. In each figure we show the results for $\mu > 0$. As expected, the region of parameter space with the lightest superpartners is excluded. This is exemplified by considering the input parameters which directly set the scale of the superpartner spectrum. In Fig. 5 we show the results in the ($M_{1/2}$, M_0) plane (Fig. (a)), and in the (M, Λ) plane (Figs. (b) and (c)). We see that in the supergravity model we exclude $M_0 < 9$ GeV and $M_{1/2} < 105$ GeV for this sign of μ. The region of parameter space with the smallest values of Λ is likewise excluded, giving the limit $\Lambda > 36(14)$ TeV in the $\mathbf{5} + \overline{\mathbf{5}}$ ($\mathbf{10} + \overline{\mathbf{10}}$) model.

These limits correspond to limits on the physical superpartner spectrum. For example, in Fig. 6 we show the results in the (m_{H^+}, $\tan\beta$) plane. The constraint from the B($B \to X_s\gamma$) measurement strongly excludes light charged Higgs masses in the $\mu > 0$ case. Depending on the model, charged Higgs masses below 240–330 GeV are excluded. As a last example, we show the excluded region in the ($m_{\tilde{q}}$, $m_{\tilde{g}}$) parameter space in Fig. 7 [f]. The squark (gluino) masses must be above 280 GeV (255 GeV) in the supergravity model. In the $\mathbf{10} + \overline{\mathbf{10}}$ gauge-mediated model the squark and gluino masses are excluded below 340 GeV. See Ref. [29] for the excluded regions of other masses and parameters.

[f] The first two generation squark masses are nearly degenerate. The squark mass plotted is actually $m_{\tilde{u}_L}$.

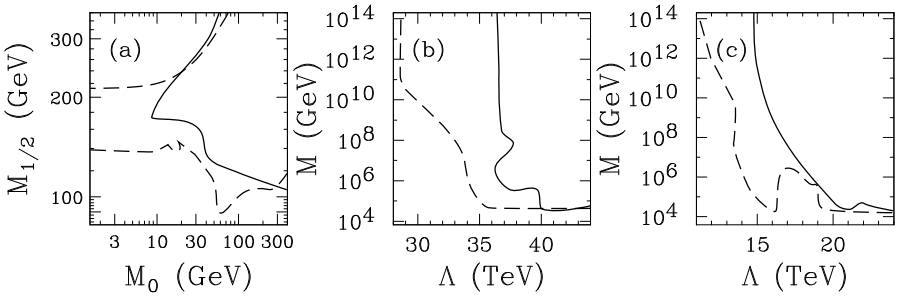

Figure 5: Excluded and non-excluded regions in the (a) supergravity model, (b) $\mathbf{5} + \overline{\mathbf{5}}$ gauge-mediated model, and (c) $\mathbf{10} + \overline{\mathbf{10}}$ gauge-mediated model, in the ($M_{1/2}$, M_0) or (M, Λ) planes, with $\mu > 0$. The region of parameter space where it is possible to find $\Delta\chi^2 > 3.84$ is bounded by the dahsed curve. The solid curve indicates the region of parameter space within which it is possible to find $\Delta\chi^2 < 3.84$. The region outside the solid curve, but inside the dashed curve, is absolutely excluded, independently of the values of any other parameters.

The results in the $\mu < 0$ case are typically not as strong, since the B($B \to X_s\gamma$) constraint is much weaker. Nevertheless, there are significant regions of parameter space excluded. In fact, for all three models under consideration we find the following bounds on the superpartner spectrum for either sign of μ:

- $m_{\tilde{q}} > 280$ GeV ,
- $m_{\tilde{g}} > 255$ GeV ,
- $m_{\tilde{\chi}_1^0} > 45$ GeV ,
- $m_{\tilde{\chi}_2^+} > 195$ GeV ,
- $m_{\tilde{e}_L} > 105$ GeV ,
- $m_h > 78$ GeV ,
- $m_H > 115$ GeV ,
- $m_A > 115$ GeV ,
- $m_{H^+} > 140$ GeV .

In each of these cases the χ^2 analysis gives us information about the particle spectrum beyond that which we can currently obtain from direct particle searches. This provides an example of an interesting and useful application of the renormalization we derived in the previous section.

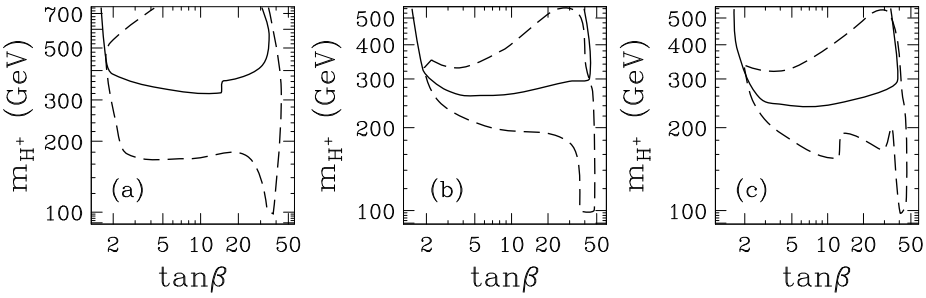

Figure 6: Excluded and non-excluded regions in the (charged Higgs mass, $\tan\beta$) plane, in the (a) supergravity model, (b) $\mathbf{5}+\overline{\mathbf{5}}$ gauge-mediated model, and (c) $\mathbf{10}+\overline{\mathbf{10}}$ gauge-mediated model. The curves are as described in Fig. 5.

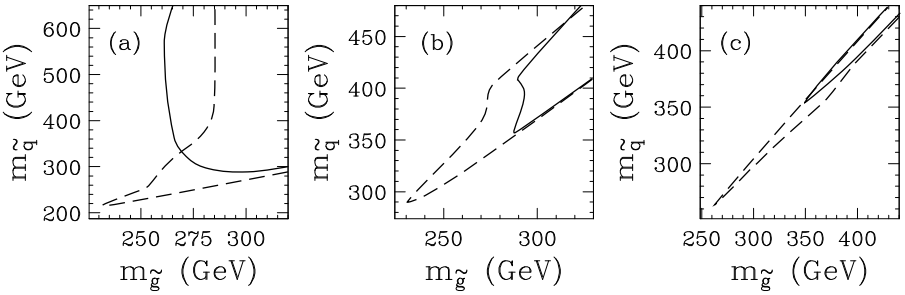

Figure 7: Excluded and non-excluded regions in the (squark mass, gluino mass) plane, as in Fig. 5.

6 Conclusions

In these lectures we have reviewed the renormalization of the electroweak sector of the standard model. This renormalization applies directly to the MSSM. We reviewed the formalism which allows us to compute the supersymmetric corrections to 21 LEP and SLC observables. We discussed regularization, which is necessary to calculate the Feynman diagrams. In particular we discussed $\overline{\rm DR}$ renormalization, which utilizes the dimensional reduction regularization appropriate for supersymmetric theories. We then gave some sample calculations, and illustrated the relationship between the weak-scale threshold corrections and the renormalization group equations.

Finally we compared the predictions for thirty-one observables in three supersymmetric models with the data. We saw that the regions of parameter space with light superpartners do not give a satisfactory global fit to the data.

We adopted an exclusion criteria which led to lower bounds on the various superpartner masses and parameters. These indirect limits are a nice complement to the limits found in the ongoing direct production searches, and give us a better idea of where to, and where not to, expect supersymmetry to show up.

Acknowledgments

I thank the organizers Jon Bagger and K.T. Mahanthappa for all their work which resulted in a very smoothly run and well organized school. I acknowledge Jens Erler for his collaboration on the χ^2 analysis.

References

1. Within recent years we have seen a 3.5 σ deviation in R_b, anomalous high p_T jet production at Fermilab, anomalous 4-jet events in ALEPH data and excess events at the highest energies in HERA data. All are now consistent with the standard model.
2. S. Dimopoulos, S. Raby, and F. Wilczek, *Phys. Rev.* **D24**, 1681 (1981);
   L.E. Ibáñez and G.G. Ross, *Phys. Lett.* **105B**, 439 (1981);
   U. Amaldi *et al.*, *Phys. Rev.* **D36**, 1385 (1987);
   J. Ellis, S. Kelley, and D.V. Nanopoulos, *Phys. Lett.* **249B**, 441 (1990);
   P. Langacker and M.-X. Luo, *Phys. Rev.* **D44**, 817 (1991);
   U. Amaldi, W. de Boer, and H. Fürstenau, *Phys. Lett.* **260B**, 447 (1991);
   P. Langacker and N. Polonsky, *Phys. Rev.* **D47**, 4028 (1993) and *ibid.* **D52**, 3081 (1995);
   P.H. Chankowski, Z. Płuciennik, and S. Pokorski, *Nucl. Phys.* **B439**, 23 (1995);
   J. Bagger, K. Matchev, and D. Pierce, *Phys. Lett.* **348B**, 443 (1995).
3. J.C. Collins, *Renormalization* (Cambridge University Press, Cambridge, 1984).
4. S. Kiyoura, M.M. Nojiri, D.M. Pierce, Y. Youichi, `hep-ph/9803210`, *Phys. Rev.* **D** (1998), in press.
5. J.A. Grifols and J. Sola, *Phys. Lett.* **137B**, 257 (1984); *ibid. Nucl. Phys.* **B253**, 47 (1985).
   P.H. Chankowski, A. Dabelstein, W. Hollik, W.M. Mösle, S. Pokorski and J. Rosiek, *Nucl. Phys.* **B417**, 101 (1994).
6. D.M. Pierce, J.A. Bagger, K. Matchev, and R.-J. Zhang, *Nucl. Phys.* **B491**, 3 (1997).

7. G. Degrassi, S. Fanchiotti and A. Sirlin, *Nucl. Phys.* **B351**, 49 (1991), and references therein.
8. G. 't Hooft and M. Veltman, *Nucl. Phys.* **B44**, 189 (1972);
C.G. Bollini and J.J. Giambiagi, *Phys. Lett.* **40B**, 566 (1972);
J.F. Ashmore, *Nuovo Cimento Lett.* **4**, 289 (1972); G.M. Cicuta and E. Montaldi, *Nuovo Cimento Lett.* **4**, 329 (1972).
9. W. Siegel, *Phys. Lett.* **84B**, 193 (1979);
D.M. Capper, D.R.T. Jones and P. van Nieuwenhuizen, *Nucl. Phys.* **B167**, 479 (1980);
I. Jack, D.R.T. Jones, S.P. Martin, M.T. Vaughn and Y. Yamada, *Phys. Rev.* **D50**, 5481 (1994).
10. I. Jack and D.R.T. Jones, `hep-ph/9707278`.
11. Thanks to M. Spira for bringing this point to my attention.
12. W. Beenakker, H. Kuijf, W.L. van Neerven and J. Smith, *Phys. Rev.* **D40**, 54 (1989).
13. G. Passarino, M. Veltman, *Nucl. Phys.* **B160**, 151 (1979).
14. G. 't Hooft and M. Veltman, *Nucl. Phys.* **B153**, 365 (1979);
B.A. Kniehl, *Nucl. Phys.* **B352**, 1 (1991).
15. G.J. van Oldenborgh and J.A.M. Vermaseren, *Z. Phys.* **C46**, 425 (1990);
G.J. van Oldenborgh, *Comp. Phys. Comm.* **66**, 1 (1991).
16. M. Boulware and D. Finnell, *Phys. Rev.* **D44**, 2054 (1991);
J.D. Wells, C. Kolda and G.L. Kane, *Phys. Lett.* **338B**, 219 (1994);
P.H. Chankowski and S. Pokorski, *Nucl. Phys.* **B475**, 3 (1996).
17. CDF Collaboration: F. Abe *et al.*, *Phys. Rev. Lett.* **75**, 11 (1995), *Phys. Rev.* **D52**, 4784 (1995), and R.G. Wagner, talk presented at the 5th International Conference on Physics Beyond the Standard Model, Balholm (1997);
DØ Collaboration: S. Abachi *et al.*, *Phys. Rev. Lett.* **77**, 3309 (1996), and B. Abbott *et al.*, preprint Fermilab–Conf–97–354–E, submitted to the XVIII International Symposium on Lepton Photon Interactions, Hamburg (1997);
UA2 Collaboration: S. Alitti *et al.*, *Phys. Lett.* **276B**, 354 (1992);
the LEP Collaborations ALEPH, DELPHI, L3, OPAL, the LEP Electroweak Working Group, and the SLD Heavy Flavour Group: D. Abbaneo *et al.*, preprint LEPEWWG/97–02.
18. CDF Collaboration: F. Abe *et al.*, *Phys. Rev. Lett.* **79**, 1992 (1997), and S. Leone, talk presented at the High-Energy Physics International Euroconference on Quantum Chromodynamics (QCD 97), Montpellier (1997);
DØ Collaboration: S. Abachi *et al.*, *Phys. Rev. Lett.* **79**, 1197 (1997),

and B. Abbott *et al.*, e-print `hep-ex/9706014`.
19. N.H. Edwards, S.J. Phipp, P.E.G. Baird, and S. Nakayama, *Phys. Rev. Lett.* **74**, 2654 (1995);
P.A. Vetter, *et al.*, *Phys. Rev. Lett.* **74**, 2658 (1995);
C.S. Wood *et al.*, *Science* **275**, 1759 (1997).
20. CCFR Collaboration: K.S. McFarland *et al.*, e-print `hep-ex/9701010`;
CDHS Collaboration: H. Abramowicz *et al.*, *Phys. Rev. Lett.* **57**, 298 (1986), and A. Blondel *et al.*, *Z. Phys.* **C45**, 361 (1990);
CHARM Collaboration: J.V. Allaby *et al.*, *Phys. Lett.* **117B**, 446 (1986) and *Z. Phys.* **C36**, 611 (1987).
21. CHARM II Collaboration: P. Vilain *et al.*, *Phys. Lett.* **335B**, 246 (1994); for earlier results see J. Panman in *Precision Tests of the Standard Electroweak Model*, ed. P. Langacker (World Scientific, Singapore, 1995).
22. CLEO Collaboration: M.S. Alam *et al.*, *Phys. Rev. Lett.* **74**, 2885 (1995).
23. R. Alemany, M. Davier, and A. Höcker, *Eur. Phys. J.* **C2**, 123 (1998).
Other determinations of $\Delta\alpha^{(5)}_{\rm had}$ appear in
H. Burkhardt and B. Pietrzyk, *Phys. Lett.* **356B**, 398 (1995);
S. Eidelman and F. Jegerlehner, *Z. Phys.* **C67**, 585 (1995);
A.D. Martin and D. Zeppenfeld, *Phys. Lett.* **345B**, 558 (1995);
M.L. Swartz, *Phys. Rev.* **D53**, 5268 (1996);
M. Davier and A. Höcker, `hep-ph/9801361` and `hep-ph/9805470`;
J.H. Kühn and M. Steinhauser, `hep-ph/9802241`;
S. Groote, J.G. Körner, K. Schilcher and N.F. Nasrallah, `hep-ph/9802374`;
J. Erler, `hep-ph/9803453`.
24. For recent reviews see P. N. Burrows, *Acta Phys. Polon.* **B28**, 701 (1997), and I. Hinchliffe, *Quantum Chromodynamics*, in R.M. Barnett *et al.*, *Phys. Rev.* **D54**, 1 (1996).
25. S.P. Li and M. Sher, *Phys. Lett.* **140B**, 339 (1984);
Y. Okada, M. Yamaguchi, and T. Yanagida, *Prog. Theo. Phys.* **D85**, 1 (1991), *Phys. Lett.* **262B**, 54 (1991);
J. Ellis, G. Ridolfi and F. Zwirner, *Phys. Lett.* **257B**, 83 (1991);
J. Ellis, G. Ridolfi and F. Zwirner, *Phys. Lett.* **262B**, 477 (1991);
H.E. Haber and R. Hempfling, *Phys. Rev. Lett.* **66**, 1815 (1991);
R. Barbieri, M. Frigeni and M. Caravaglios, *Phys. Lett.* **263B**, 233 (1991);
P.H. Chankowski, preprint IFT-7-91-WARSAW (1991);
J.R. Espinosa and M. Quirós, *Phys. Lett.* **266B**, 389 (1991);
J.L. Lopez and D.V. Nanopoulos, *Phys. Lett.* **266B**, 397 (1991);

D.M. Pierce, A. Papadopoulos and S.B. Johnson, *Phys. Rev. Lett.* **68**, 3678 (1992);
M. Drees and M.M. Nojiri *Phys. Rev.* **D45**, 2482 (1992);
A. Brignole, *Phys. Lett.* **281B**, 284 (1992);
J. Kodaira, Y. Yasui and K. Sasaki, *Phys. Rev.* **D50**, 7035 (1994);
R. Hempfling and A.H. Hoang, *Phys. Lett.* **331B**, 99 (1994);
A.V. Gladyshev and D.I. Kazakov, *Mod. Phys. Lett.* **AA10**, 3129 (1995);
J.A. Casas, J.R. Espinosa, M. Quiros and A. Riotto, *Nucl. Phys.* **B436**, 3 (1995) [E: **B439**, 466 (1995)];
M. Carena, J.R. Espinosa, M. Quiros and C.E.M. Wagner, *Phys. Lett.* **355B**, 209 (1995);
M. Carena, M. Quiros and C.E.M. Wagner, *Nucl. Phys.* **B461**, 407 (1996);
A.V. Gladyshev, D.I. Kazakov, W. de Boer, G. Burkart and R. Ehret, *Nucl. Phys.* **B498**, 3 (1997);
H.E. Haber, `hep-ph/9707213`;
H.E. Haber, R. Hempfling and A.H. Hoang, *Z. Phys.* **C75**, 539 (1997);
S. Heinemeyer, W. Hollik and G. Weiglein, `hep-ph/9803277`.

26. See H.P. Nilles, *Phys. Rep.* **110**, 1 (1984) for a review and references.

27. M. Dine, W. Fischler, and M. Srednicki, *Nucl. Phys.* **B189**, 575 (1981);
S. Dimopoulos and S. Raby, *Nucl. Phys.* **B192**, 353 (1981);
M. Dine and M. Srednicki, *Nucl. Phys.* **B202**, 238 (1982);
L. Alvarez-Gaumé, M. Claudson, and M.B. Wise, *Nucl. Phys.* **B207**, 96 (1982);
C.R. Nappi and B.A. Ovrut, *Phys. Lett.* **113B**, 175 (1982);
I. Affleck, M. Dine, and N. Seiberg, *Nucl. Phys.* **B256**, 557 (1985);
M. Dine and W. Fischler, *Phys. Lett.* **110B**, 227 (1992);
M. Dine and A.E. Nelson, *Phys. Rev.* **D48**, 1277 (1993);
M. Dine, A.E. Nelson, and Y. Shirman, *Phys. Rev.* **D51**, 1362 (1995).

28. K. Inoue, A. Kakuto, H. Kamatsu and S. Takeshita, *Prog. Theo. Phys.* **D68**, 927 (1982);
L. Alvarez-Gaumé, J. Polchinkski and M.B. Wise, *Nucl. Phys.* **B221**, 495 (1983);
J. Ellis, J.S. Hagelin, D.V. Nanopoulos and K. Tamvakis, *Phys. Lett.* **125B**, 275 (1983);
L.E. Ibañez and C. Lopez, *Nucl. Phys.* **B233**, 511 (1984);
L.E. Ibañez, C. Lopez and C. Muñoz, *Nucl. Phys.* **B250**, 218 (1985).

29. J. Erler and D.M. Pierce, `hep-ph/9801238`, *Nucl. Phys.* **B** (1998), in press.

30. M.E. Peskin and T. Takeuchi, *Phys. Rev. Lett.* **65**, 964 (1990) and *Phys. Rev.* **D46**, 381 (1992).

	measurement	SM	pull
M_Z [GeV]	91.1867 ± 0.0020	91.1867	0.0
Γ_Z [GeV]	2.4948 ± 0.0025	2.4959	-0.4
$\sigma_{\rm had}$[nb]	41.486 ± 0.053	41.478	0.2
R_e	20.757 ± 0.056	20.744	0.2
R_μ	20.783 ± 0.037	20.744	1.1
R_τ	20.823 ± 0.050	20.789	0.7
$A^{FB}(e)$	0.0160 ± 0.0024	0.0163	-0.1
$A^{FB}(\mu)$	0.0163 ± 0.0014	0.0163	0.0
$A^{FB}(\tau)$	0.0192 ± 0.0018	0.0163	1.6
$\mathcal{P}(\tau)$	0.1411 ± 0.0064	0.1476	-1.0
$\mathcal{P}^{FB}(\tau)$	0.1399 ± 0.0073	0.1476	-1.1
$\sin^2\theta^e_{\rm eff}(Q^{FB})$	0.2322 ± 0.0010	0.2315	0.8
R_b	0.2170 ± 0.0009	0.2158	1.3
R_c	0.1734 ± 0.0048	0.1722	0.2
$A^{FB}(b)$	0.0984 ± 0.0024	0.1035	-2.1
$A^{FB}(c)$	0.0741 ± 0.0048	0.0739	0.0
$A^{FB}_{LR}(b)$	0.900 ± 0.050	0.935	-0.7
$A^{FB}_{LR}(c)$	0.650 ± 0.058	0.668	-0.3
A_e	0.1548 ± 0.0033	0.1476	2.2
$A^{FB}_{LR}(\mu)$	0.102 ± 0.034	0.148	-1.3
$A^{FB}_{LR}(\tau)$	0.195 ± 0.034	0.148	1.4
M_W [GeV]	80.430 ± 0.076	80.386	0.6
m_t [GeV]	175 ± 5	172	0.6
Q_W(Cs)	-72.11 ± 0.93	-73.11	1.1
Q_W(Tl)	-114.8 ± 3.7	-116.7	0.5
κ(DIS)	0.581 ± 0.0039	0.583	-0.7
$g_V^{\nu e}$	-0.041 ± 0.015	-0.0396	-0.1
$g_A^{\nu e}$	-0.507 ± 0.014	-0.5064	0.0
$\lg(B(B \to X_s\gamma))$	-8.49 ± 0.45	-7.99	-1.1
$\Delta\alpha^{(5)}_{\rm had}$	0.02817 ± 0.00062	0.02817	0.0
$\alpha_s(M_Z)$	0.118 ± 0.003	0.1195	-0.5

Table 1: Results of a global fit to the standard model. For each observable, we list the experimental result, the best fit result in the SM, and the pull. The pull is the difference between the measured value and the prediction, divided by the error.